NAVAL POSTGRADUATE SCHOOL

MONTEREY, CALIFORNIA

THESIS

INVESTIGATIONS OF PHYSICS LECTURE DEMONSTRATIONS: TWO-BULLET PROBLEM AND PARAMETRIC EXCITATION OF U-TUBE OSCILLATIONS

by

Hannah S. Steiner

June 2020

Thesis Advisor: Bruce C. Denardo
Co-Advisor: Andres Larraza

Approved for public release. Distribution is unlimited.

THIS PAGE INTENTIONALLY LEFT BLANK

REPORT DOCUMENTATION PAGE			*Form Approved OMB No. 0704-0188*

Public reporting burden for this collection of information is estimated to average 1 hour per response, including the time for reviewing instruction, searching existing data sources, gathering and maintaining the data needed, and completing and reviewing the collection of information. Send comments regarding this burden estimate or any other aspect of this collection of information, including suggestions for reducing this burden, to Washington headquarters Services, Directorate for Information Operations and Reports, 1215 Jefferson Davis Highway, Suite 1204, Arlington, VA 22202-4302, and to the Office of Management and Budget, Paperwork Reduction Project (0704-0188) Washington, DC, 20503.

1. AGENCY USE ONLY *(Leave blank)*	**2. REPORT DATE** June 2020	**3. REPORT TYPE AND DATES COVERED** Master's thesis

4. TITLE AND SUBTITLE
INVESTIGATIONS OF PHYSICS LECTURE DEMONSTRATIONS: TWO-BULLET PROBLEM AND PARAMETRIC EXCITATION OF U-TUBE OSCILLATIONS

5. FUNDING NUMBERS

6. AUTHOR(S) Hannah S. Steiner

7. PERFORMING ORGANIZATION NAME(S) AND ADDRESS(ES)
Naval Postgraduate School
Monterey, CA 93943-5000

8. PERFORMING ORGANIZATION REPORT NUMBER

9. SPONSORING / MONITORING AGENCY NAME(S) AND ADDRESS(ES)
N/A

10. SPONSORING / MONITORING AGENCY REPORT NUMBER

11. SUPPLEMENTARY NOTES The views expressed in this thesis are those of the author and do not reflect the official policy or position of the Department of Defense or the U.S. Government.

12a. DISTRIBUTION / AVAILABILITY STATEMENT
Approved for public release. Distribution is unlimited.

12b. DISTRIBUTION CODE
A

13. ABSTRACT (maximum 200 words)

Lecture demonstrations strongly convey physics concepts and theories. In addition, realistic issues arise that are often not in a model theory. Investigations of lecture demonstrations are published in scholarly journals and are Navy-relevant due to use in classrooms. We investigate two lecture demonstrations. One is the "two-bullet problem," where a body is released from rest at a height, and another is simultaneously projected at the same height. In a vacuum, it is well known that both strike the floor simultaneously. For the common case of quadratic drag, however, the dropped body is predicted to strike the floor first. We develop a classroom demonstration that clearly exhibits the effect, but the result is suspect because numerical simulations show that the time difference is too small to be clearly discernible. Arguments to resolve the inconsistency are made. In the other demonstration, we describe the first successful parametric excitation of oscillations of the liquid in a U-tube. This is difficult to achieve due to a large drive amplitude threshold. Only a nonlinearity can limit parametric growth and thus lead to steady-state motion, but the observed motion is in the Hooke's law regime, and the dissipation is very nearly linear. Possible reasons for the steady-state motion are discussed. Also surprising is that the free decay transitions from one damping parameter to a greater one at small amplitudes. We propose a possible reason for this behavior.

14. SUBJECT TERMS physics, demonstrations, two bullet, U-tube, non-linear systems	**15. NUMBER OF PAGES** 85
	16. PRICE CODE

17. SECURITY CLASSIFICATION OF REPORT	**18. SECURITY CLASSIFICATION OF THIS PAGE**	**19. SECURITY CLASSIFICATION OF ABSTRACT**	**20. LIMITATION OF ABSTRACT**
Unclassified	Unclassified	Unclassified	UU

NSN 7540-01-280-5500

Standard Form 298 (Rev. 2-89)
Prescribed by ANSI Std. 239-18

THIS PAGE INTENTIONALLY LEFT BLANK

Approved for public release. Distribution is unlimited.

INVESTIGATIONS OF PHYSICS LECTURE DEMONSTRATIONS: TWO-BULLET PROBLEM AND PARAMETRIC EXCITATION OF U-TUBE OSCILLATIONS

Hannah S. Steiner
Ensign, United States Navy
BS, U.S. Naval Academy, 2019

Submitted in partial fulfillment of the
requirements for the degree of

MASTER OF SCIENCE IN PHYSICS

from the

NAVAL POSTGRADUATE SCHOOL
June 2020

Approved by: Bruce C. Denardo
Advisor

Andres Larraza
Co-Advisor

Kevin B. Smith
Chair, Department of Physics

THIS PAGE INTENTIONALLY LEFT BLANK

ABSTRACT

Lecture demonstrations strongly convey physics concepts and theories. In addition, realistic issues arise that are often not in a model theory. Investigations of lecture demonstrations are published in scholarly journals and are Navy-relevant due to use in classrooms. We investigate two lecture demonstrations. One is the "two-bullet problem," where a body is released from rest at a height, and another is simultaneously projected at the same height. In a vacuum, it is well known that both strike the floor simultaneously. For the common case of quadratic drag, however, the dropped body is predicted to strike the floor first. We develop a classroom demonstration that clearly exhibits the effect, but the result is suspect because numerical simulations show that the time difference is too small to be clearly discernible. Arguments to resolve the inconsistency are made. In the other demonstration, we describe the first successful parametric excitation of oscillations of the liquid in a U-tube. This is difficult to achieve due to a large drive amplitude threshold. Only a nonlinearity can limit parametric growth and thus lead to steady-state motion, but the observed motion is in the Hooke's law regime, and the dissipation is very nearly linear. Possible reasons for the steady-state motion are discussed. Also surprising is that the free decay transitions from one damping parameter to a greater one at small amplitudes. We propose a possible reason for this behavior.

THIS PAGE INTENTIONALLY LEFT BLANK

TABLE OF CONTENTS

I. INTRODUCTION 1
A. IMPORTANCE OF PHYSICS LECTURE DEMONSTRATIONS 1
B. GOALS OF THE THESIS 3

II. TWO-BULLET PROBLEM 7
A. INTRODUCTIONS 7
1. Vacuum and Linear Drag 9
2. Resistive Force of Constant Magnitude 10
3. Quadratic Drag 11
B. EXPERIMENTS 14
1. Apparatus 14
2. Approximate Effect of Small Angle of Inclination 17
3. Dropped and Projected Balls 19
4. Drag Coefficient of Styrofoam Ball 24
C. COMPUTER SIMULATIONS 28
1. Feasibility of Lecture Demonstration 28
2. Bullets 33
3. Inclusion of Buoyancy 33
D. CONCLUSIONS AND FUTURE WORK 36

III. PARAMETRIC EXCITATION OF U-TUBE OSCILLATIONS 39
A. BACKGROUND AND MOTIVATION 39
B. APPARATUS 42
1. Linear Variable Differential Transformer (LVDT) 42
2. Selection of Subwoofer 44
3. Construction of U-Tube Apparatus 46
C. FREE-DECAY MEASUREMENTS 48
D. DRIVE AMPLITUDE THRESHOLDS 51
1. Excitation from Rest 51
2. Maintenance of Steady-State Oscillations 57
E. CONCLUSIONS AND FUTURE WORK 59

IV. SUMMARY 63
A. TWO-BULLET PROBLEM 63
B. PARAMETRIC EXCITATION OF U-TUBE OSCILLATIONS 65

APPENDIX. EULER'S METHOD SIMULATION 67

LIST OF REFERENCES 69

INITIAL DISTRIBUTION LIST 71

LIST OF FIGURES

Figure 1. Michael Faraday's Christmas Lecture Demonstration. Source: Science Source (1856). 1

Figure 2. Two-Bullet Problem....7

Figure 3. Drop-Launch Apparatus Marketed by 3B Scientific Company. Source: 3B Scientific Company (2019). 15

Figure 4. Drop-Launch Apparatus Marketed by Pasco. Source: Pasco (2019).....15

Figure 5. Mounted Drop-Launch Mechanism. 17

Figure 6. 1-D Graph of Experimental Times of Flight....20

Figure 7. Top View of Drop-Launch Apparatus. 21

Figure 8. Photogate Apparatus. 22

Figure 9. Upper and Lower Parts of Apparatus to Determine the Drag Coefficient of a Styrofoam Ball. 26

Figure 10. Data from Freefall Experiment. 27

Figure 11. Time Difference (Top) and Range (Bottom) versus Quadratic Drag Coefficient for Various Initial Velocities. 31

Figure 12. Projectile Simulation Results for No Drag and for Quadratic Drag. 32

Figure 13. Parametric Excitation of a Simple Pendulum. 39

Figure 14. Parametrically Driven Liquid in a U-tube. 41

Figure 15. Calibration Graph for the LVDT. 43

Figure 16. Parametrically Driven U-tube Apparatus....47

Figure 17. Semilogarithmic Plot of Free Decay Amplitude Data of U-tube Oscillations 49

Figure 18. U-tube Apparatus with a Hand Pump for Displacement. 54

Figure 19. Drive Amplitude Thresholds as a Function of Drive Frequency. 55

THIS PAGE INTENTIONALLY LEFT BLANK

LIST OF TABLES

Table 1. Relative Times-of-Flight for the Two-Bullet Problem for Different Power-Law Resistive Forces. Adapted from Burris et al. (2018). 8

Table 2. Parameters of Various Balls 14

Table 3. Various Low Frequency Loudspeakers Tested for Use as Parametric Drive of U-Tube 45

THIS PAGE INTENTIONALLY LEFT BLANK

I. INTRODUCTION

A. IMPORTANCE OF PHYSICS LECTURE DEMONSTRATIONS

The importance of the use of physics lecture demonstrations to help people grasp concepts in physics has been recognized for at least two centuries. In 1825, British physicist Michael Faraday instituted the Christmas lecture series at the Royal Institution in London, and the series continues to this day. Faraday delivered a total of 19 lectures, the first in 1827 and the last in 1860, and he often performed demonstrations (Figure 1).

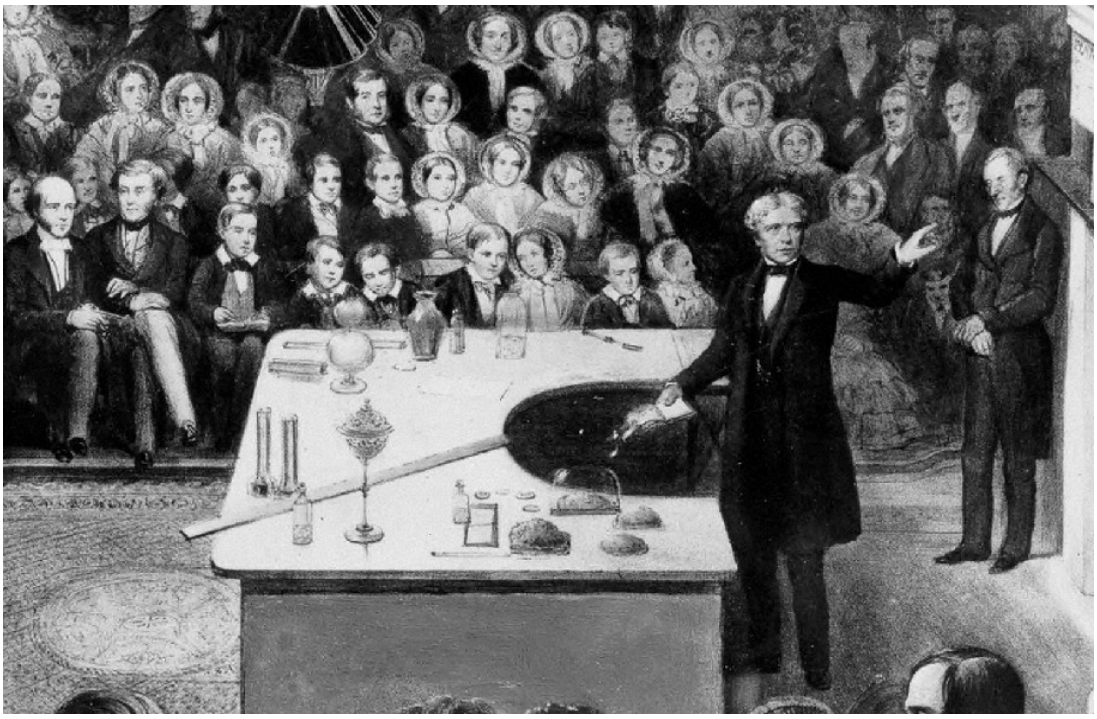

Figure 1. Michael Faraday's Christmas Lecture Demonstration. Source: Science Source (1856).

Lecture demonstrations strongly and often dramatically convey physics concepts and theories. Demonstrations are thus naturally very popular among students. In addition, realistic effects that are not in model theories frequently arise in demonstrations, which leads to classroom discussions. This is especially true at the Naval Postgraduate School

(NPS), where the students typically have substantial experience with practical physical systems.

Investigations of lecture demonstrations are published in scholarly journals and books, and are automatically Navy-relevant due to use of the demonstrations in NPS classrooms. In addition, local and national meetings of the American Association of Physics Teachers always have sessions in which demonstrations are presented, and this is undoubtedly true for educational physics societies around the world.

By their nature, physics lecture demonstrations are nearly always simple and done qualitatively in lectures. However, a demonstration that is investigated in a thesis, and is thus under consideration for publication, should be treated as a genuine experiment, where data are gathered and compared to theory. The reason for quantitative investigations is to establish whether or not the demonstration is actually behaving in accord with theory. Just as in forefront research, the results can be surprising and can lead to discoveries.

Many major international efforts have been made in STEM education (science, technology, engineering, and mathematics) since the early 2000s, when the acronym was introduced by the National Science Foundation in the U.S. The advent of STEM has caused physics demonstrations to become even more important as means of making physics accessible to students.

The Department of Defense recognizes the necessity of STEM both for its problem solving and critical thinking skills along with the technological advances. Naval STEM is a program under the Office of Naval Research Science and Technology in support of the Department of the Navy's education and outreach programs (Office of Naval Research, n.d.). One such program is the United States Naval Academy's Summer STEM program (USNA Admissions, n.d.). This program invites high school students to reside at the campus for a week of lectures, demonstrations, and other forms of hands on learning regarding various STEM topics. The program facilitates higher thinking and problem solving in its attendees while promoting the Naval Academy as a forefront undergraduate program.

In the next section, we discuss the basic goals of this thesis. It should be noted that the body of the thesis (Chapters 2 and 3) consists of essentially two separate sub-theses on different physics lecture demonstrations. Each of these chapters has its own extensive introduction and body, as well as conclusions and future work. Precedents for this natural structure are in previous theses on educational research in physics lecture demonstrations (Emerson, 2015; Garlington & Martinez, 2017; Khan, 2015).

B. GOALS OF THE THESIS

We investigate two possible physics lecture demonstrations. Our basic goal is to create apparatuses that can readily be used in the classroom, and that convincingly show one or more phenomena in physics. Extensive searches of the scientific literature on the two demonstrations did not reveal that these goals had been met by any other investigators.

The first demonstration is called the "two-bullet problem." Two identical bodies (not necessarily bullets) are initially at the same height. One body is released from rest, and the other is simultaneously projected horizontally. Which strikes the ground first? If the drag due to the air is negligible, the answer should be well-known to any student who has taken an introductory mechanics course in physics: They strike the ground at the *same* time, regardless of the initial velocity of the projected body. The reason is that the motion of the dropped body in this case is *identical* to vertical motion of the projected body. This occurs because the vertical and horizontal motions of the projected body are *uncoupled*; that is, they do not influence each other. So the bodies must strike the ground at the same time.

There exist several different commercial apparatuses for classroom use. These are simple and inexpensive, and use steel balls as the bodies. The drag due to the air is negligible in these cases, and the balls are indeed observed to strike the floor at the same time.

The issue is what happens in more realistic cases in which the drag is *not* negligible. We consider the common case of a drag force that is proportional to the square of the velocity of a body ("quadratic drag"). We show in Ch. II that the dropped ball should strike the floor *before* the horizontally-projected ball, which occurs due to the coupling of the

drag in the vertical and horizontal motions. Our goal is to convincingly demonstrate this effect. To increase the effect of the drag, we use Styrofoam balls. To ensure that we are not observing one or more experimental artifacts, we do computer simulations with quadratic drag. As we show, the results are surprising. We also compare our simulations to an experiment done with actual fired and dropped bullets in a TV episode of MythBusters.

The second demonstration involves what is called *parametric excitation*, which is one of the three types of driving mechanisms that can excite and maintain the motion of a damped oscillator. Parametric excitation is seldom taught in courses, but it can and should be briefly discussed and demonstrated. The other two types of drives are the standard *direct drive*, which is universally taught in courses, and a *maintained* or *self-sustained drive*, which is seldom taught.

Consider any parameter upon which the natural frequency of an oscillator depends. Parametric excitation can occur when the parameter is modulated in time. The optimum parametric drive frequency is twice the natural frequency. One standard example of parametric excitation is to use hands to modulate the length of a simple pendulum. The cord of the pendulum passes through a large eyelet formed by the thumb and forefinger of one hand, and the other hand oscillates the upper end of the cord in and out. The other standard example is to modulate the gravitational acceleration of a simple pendulum, which is simply achieved by using a hand to vertically oscillate the support of a pendulum. In the frame of reference of the support, the acceleration due to gravity is modulated.

Parametric excitation has properties that are fundamentally different from direct excitation. Growth of the response amplitude only occurs above drive amplitude threshold. In addition, the growth is exponential in time, and can only be limited by nonlinearity. The phenomenon can thus be described as a kind of “all or nothing.” The effect can occur when waves striking ships cause vertical oscillations which then parametrically drive rolling oscillations. One mode parametrically drives another mode, and the result can be a *parametric instability*. Due to the exponential growth, this instability has caused extensive damage on ships.

U-tubes are used as manometers (to measure pressure) and also on ships to damp rolling motion. Our goal is to create a lecture demonstration apparatus in which U-tube oscillations are parametrically excited and maintained by vertical displacement of the tube. One of our motivations is to extend parametric excitation demonstrations beyond pendulums, to show the generality of the phenomenon. Another motivation is to visually show that only a nonlinearity limits the growth, which cannot convincingly be done with pendulums. U-tubes are *linear* (Hooke's law occurs) until ends of liquid enter rounded region. For a drive just above threshold, growth should initially accelerate slowly and then dramatically saturate when the ends of the liquid enter the rounded regions. Another goal is to map the boundary in drive plane (drive amplitude vs. drive frequency) above which excitation occurs, and compare results to theory. However, a fundamental problem is that all but very large U-tubes have substantial damping, which increases the drive amplitude threshold for excitation. As we show, meeting the threshold in this case turns out to be very challenging!

THIS PAGE INTENTIONALLY LEFT BLANK

II. TWO-BULLET PROBLEM

A. INTRODUCTIONS

The "two-bullet problem" is well known in physics, and to a significant extent even to the public at large. A bullet is released from rest at some height (Figure 2). At the same time and initial height, an identical bullet is shot horizontally. Which bullet strikes the ground first?

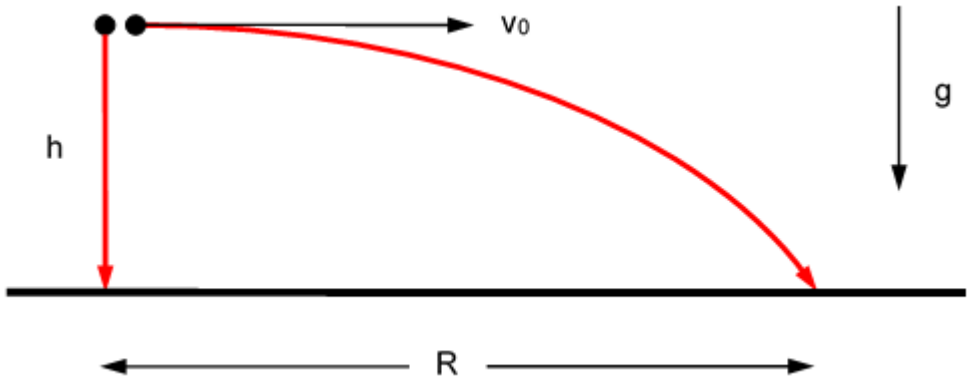

Two identical bodies are initially at the same height above the ground. One body is released from rest, and the other body is simultaneously projected horizontally. Which body strikes the ground first?

Figure 2. Two-Bullet Problem.

It is elementary to show (Section A.1) that, in a vacuum, the two bodies strike the ground at the same time. Keeports (1997) showed that this also occurs when the drag is linear (Section A.1). For quadratic drag, Keeports showed that the dropped body strikes the ground before the projected body (Section A.3). Burris et al. (2018) investigated the case of a resistive force of constant magnitude, which occurs for the standard model of kinetic friction, where the bodies slide on an inclined plane. In this case, the projected body reaches the bottom *before* the dropped body (Section A.2). The results for the three power law cases v^n, where n = 0, 1, and 2, are summarized in Table 1.

Table 1. Relative Times-of-Flight for the Two-Bullet Problem for Different Power-Law Resistive Forces. Adapted from Burris et al. (2018).

resistive force	upward component of resistive force on projected body	relative times-of-flight
$\propto v^2$	$\propto v_y(v_x^2 + v_y^2)^{1/2}$	dropped body lands first
$\propto v$	$\propto v_y$	simultaneous
$\propto v^0$ (= const)	$\propto v_y/(v_x^2 + v_y^2)^{1/2}$	projected body lands first

The speed of the projectile is v, where the components of the velocity are v_x and v_y. Consideration of the upward components of the resistive force explains the relative times-of-flight, as discussed in Sections A.1, A.2, and A.3.

Keeports (1997) first attempted but failed to experimentally demonstrate the quadratic drag result, but he did not sufficiently elaborate on his various attempts. He then turned to computer simulations, and concluded that the effect would be readily observable only for bodies with substantial buoyancy, where the average density is only marginally greater than air. In the end, Keeports developed a demonstration with a very large balloon that was partially filled with helium such that the average density was only a small amount greater than the density of air. However, separate times-of-flight of the dropped and horizontally-projected balloon had to be measured.

Our main goal is to develop a lecture demonstration that simply and convincingly shows that a dropped body strikes the floor or table before a projected body. We desire a side-by-side simultaneous comparison, so that the times-of-flight do not have to be measured. Because Keeports relied on tables of computer simulations for only a few values of the parameters, and did not produce any graphs, we are concerned that he might have missed a set of parameters that meet our requirements.

We consider the cases of a vacuum and linear drag in Section A.1, a resistive force of constant magnitude in Section A.2, and quadratic drag in Section A.3. We discuss a lecture demonstration and related experiments in Section B. Results of computer simulations are presented in Section C. Conclusions and future work are stated in Section D.

1. Vacuum and Linear Drag

We first consider a vacuum. The motion of either body is given by

$$\frac{d\mathbf{v}}{dt} = \mathbf{g}, \tag{A.1}$$

where **v** is the vector velocity, t is the time, and **g** is the constant vector acceleration due to gravity. The motion of the dropped body is given by dv/dt = g, which yields the velocity v = gt. The downward displacement measured from the initial location is then

$$y = \frac{1}{2}gt^2 \quad \text{so} \quad h = \frac{1}{2}gT^2,$$

where T is the time-of-flight, which is given by

$$T = \sqrt{\frac{2h}{g}}. \tag{A.2}$$

From Equation (A.1), the x and y equations of motion of the projected body are

$$\frac{dv_x}{dt} = 0 \quad \text{and} \quad \frac{dv_y}{dt} = g.$$

The x and y equations are *uncoupled*; in particular, the vertical motion is *identical* to that of the dropped body. *Both bodies must then strike the ground at the same time.* The common time-of-flight is given by Equation (A.2).

We now include linear drag. The equation of motion of either body is

$$\frac{d\mathbf{v}}{dt} = \mathbf{g} - \alpha\mathbf{v},$$

where $\alpha > 0$. The equation of motion for the dropped body is

$$\frac{dv}{dt} = g - \alpha v, \tag{A.3}$$

and the x and y equations of motion of the projected body are

$$\frac{dv_x}{dt} = -\alpha v_x \quad \text{and} \quad \frac{dv_y}{dt} = g - \alpha v_y.$$

As in the case of a vacuum, the x and y motions are *uncoupled*; in particular, the y motion is *identical* to that of the dropped body in Equation (A.3). Hence, the bodies must strike the ground at the *same* time. Note that, due to the upward component of the drag force, the time-of-flight will be greater than that in Equation (A.2) which is for a vacuum.

2. Resistive Force of Constant Magnitude

For a body sliding on an inclined plane, the standard model of kinetic friction is that the resistive force has constant magnitude. The motion for either body is then given by

$$\frac{dv}{dt} = g' - \beta\frac{v}{v},$$

where the $\beta > 0$, and where the magnitude of the downward acceleration due to gravity in the plane is $g' = g\sin(\theta)$, where θ is the angle of inclination of the plane. The equation holds provided that the body is moving; that is, that static friction does not occur. For a body that is moving solely in the y direction directly down the plane, the equation of motion is then

$$\frac{dv}{dt} = g' - \beta. \tag{A.4}$$

For a body that projected, the x and y equations of motion are

$$\frac{dv_x}{dt} = -\beta\frac{v_x}{\sqrt{v_x^2 + v_y^2}} \quad \text{and} \quad \frac{dv_y}{dt} = g' - \beta\frac{v_y}{\sqrt{v_x^2 + v_y^2}}.$$

Comparing the y equation of motion to the equation of motion (A.4) for the body moving directly down the plane, we observe that the magnitude of the kinetic frictional force is *less* for the projected body. Hence, the projected body will reach the bottom of the inclined plane *before* the body that is simultaneously released from rest at the same height.

3. Quadratic Drag

For the common approximation of quadratic drag, the general motion of a body is given by

$$\frac{d\mathbf{v}}{dt} = \mathbf{g} - \gamma|\mathbf{v}|\mathbf{v}, \tag{A.5}$$

where the quadratic drag factor γ is greater than zero. The motion of a dropped body is then given by

$$\frac{d\mathbf{v}}{dt} = \mathbf{g} - \gamma \mathbf{v}^2, \tag{A.6}$$

and the x and y motions of a projected body are given by

$$\frac{dv_x}{dt} = -\gamma\sqrt{v_x^2 + v_y^2}\, v_x \qquad \frac{dv_y}{dt} = g - \gamma\sqrt{v_x^2 + v_y^2}\, v_y. \tag{A.7}$$

In this case, the x and y motions are *coupled* and *nonlinear*. The equations *cannot* be analytically solved (Taylor, 2005). Qualitatively, the drag for the y motion of the projected body is *greater* than that for the dropped body, so *the dropped body strikes the ground first*.

The one-dimensional (y) case, where the initial horizontal velocity is $v_0 = 0$, can be integrated (Taylor, 2005). From the second of Equations (A.7), the equation of motion for $v_y \geq 0$ (downward direction) is given by Equation (A.6), where we use "v" instead of "v_y"

in order to distinguish this case from the two-dimensional projectile motion case. Separating the variables, integrating, and setting the initial velocity to zero, yields

$$v = \sqrt{\frac{g}{\gamma}} \tanh\left(\sqrt{\gamma g}\, t\right).$$

We set v = dy/dt, and perform a second integration from t = 0 to T_0, where T_0 is the time-of-flight for a body released from rest ($v_0 = 0$) at t = 0. Solving the resultant equation for T_0 yields

$$T_0 = \frac{1}{\sqrt{\gamma g}} \cosh^{-1}\left(e^{\gamma h}\right). \qquad \text{(A.8)}$$

In Section C of this chapter, we evaluate this expression to confirm our computer simulations for the case of a body released from rest. It can be shown that Equation (A.8) correctly reduces in the limit $\gamma \to 0$ to $T_0 = (2h/g)^{1/2}$, and in the limit $\gamma \to \infty$ to $T_0 = h/v_t$, where the terminal velocity is $v_t = (g/\gamma)^{1/2}$.

To deal with specific bodies, we now cast the quadratic drag factor γ in Equation (A.5) terms of physical parameters. In general, the quadratic drag force on a body is

$$F_D = \frac{1}{2}\rho v^2 A C_D, \qquad \text{(A.9)}$$

where ρ is the density of the fluid, v is the velocity of the body, A is the "frontal area" (the cross-sectional area perpendicular to the direction of motion), and C_D is the constant drag coefficient. From the basic equation of motion (A.5), we find that $\gamma = F_D/m$, where m is the mass of the body. Use of the drag expression (A.9) then yields

$$\gamma = \frac{1}{2m}\rho A C_D. \qquad \text{(A.10)}$$

We consider spherical bodies. The area is then $A = \pi d^2/4$, where d is the diameter, and the drag coefficient is $C_D = 0.47$. The quadratic drag factor is then

$$\gamma = \frac{0.47\pi\rho d^2}{8m}. \qquad \text{(A.11)}$$

Note that, to use the theory for experiments, we must ensure that the Reynolds number is in the regime of an approximately pure quadratic drag force.

To observe the quadratic drag effect in which a dropped ball reaches a table or the floor before a simultaneously projected identical ball, we naturally consider lightweight Styrofoam balls because the ratio of the typical drag force to the gravitational force is much greater than that for a metal. Furthermore, for balls of a specified material, the drag force is proportional to the cross-sectional area and thus the *square* of the diameter, whereas the gravitational force is proportional to the volume and thus the *cube* of the diameter. The ratio of drag force to the gravitational force is then *inversely* proportional to the diameter, so lightweight balls of sufficiently small diameter are expected show the desired effect.

However, the diameter cannot be made arbitrarily small for a number of reasons: the balls would be difficult to see in classroom, the motion of the balls would be substantially altered due to air currents, and electrostatic forces (for example, between the balls and metal in a table) may become significant. In addition, for sufficiently small balls, the drag will become *linear*, in which case they would strike a table or the floor simultaneously.

The values of γ for several different spherical bodies in air at room temperature and atmospheric pressure are listed in Table 2. Note that there is an order-of-magnitude difference in the values of γ. The larger Styrofoam ball is a nominally 1-inch diameter Styrofoam ball, which has an actual diameter of approximately d = 0.92 inches = 2.34 cm. This ball was used in our experiments (Sections B.3 and B.4).

Table 2. Parameters of Various Balls

ball	diameter d (cm)	mass m (g)	quadratic drag factor γ (m^{-1})
ping pong	4.0	2.7	0.13
Styrofoam	2.34	0.22	0.55
Styrofoam	0.80	0.01	1.4

The quantity γ is the quadratic drag factor defined by Equation (A.5), and is expressed for spherical bodies in Equation (A.11). The medium is air at room temperature and atmospheric pressure, for which the density is $\rho = 1.204 \times 10^{-3}$ g/cm^3.

B. EXPERIMENTS

1. Apparatus

We found two types of commercial educational apparatuses that demonstrate the two-bullet problem. One type is a two-dimensional mechanism that has a horizontal right-angle arm that is pivoted at its center (Figure 3). One ball rests near one end of arm, and the other ball rests near the other end. The balls are initially at the same height. A spring is attached to one end such that the arm can be cocked and fired, causing it to rotate through an angle. The arm rapidly moves away from one ball, causing it to be released from rest. At the same time, the second ball is pushed by the arm and is projected horizontally.

One ball (top of picture) is released from rest, while the other ball (bottom of picture) is simultaneously projected horizontally. The length of the base is 7 inches.

Figure 3. Drop-Launch Apparatus Marketed by 3B Scientific Company. Source: 3B Scientific Company (2019).

The other type of apparatus is a one-dimensional mechanism that consists of a horizontal rod attached to a spring such that the rod moves longitudinally (Figure 4). One ball is struck by one end of the rod. At the same time, the other end of the rod withdraws from a hole that passes through the other ball, which causes it to be released from rest.

One ball (right of picture) is released from rest, while the other ball (left of picture) is simultaneously projected horizontally. The length of the base is 11 inches.

Figure 4. Drop-Launch Apparatus Marketed by Pasco. Source: Pasco (2019).

In the apparatuses, steel balls with a typical diameter 3/4 inch or 18 mm are used. The drag force for lecture demonstrations is very much less than the gravitational force, so

the demonstrations are effectively in a vacuum. The balls should thus be heard to simultaneously strike a table or the floor, which is indeed the case if the apparatus is level.

We performed experiments with a drop-launch apparatus that is very similar to the one shown in Figure 3. Instead of steel balls, we used Styrofoam balls with a nominal diameter of 1 inch. The actual diameter is 0.92 inch, and the mass is 0.22 g. We first performed quick experiments. If the apparatus is held approximately level and high overhead, and the trigger is released, the dropped ball hits the floor well before the projected ball, as expected. The time difference is roughly 1 s. However, we noticed that the projected ball departs from the apparatus with a positive (rather than zero) angle of inclination. The angle is roughly 20^{o}. The reason that the ball is projected with a positive angle of inclination is that the height of the vertical section of the right-angle arm is *less* than the radius of the ball, so there is an upward component of the impulse on the ball in addition to the horizontal component.

We then made several improvements in the apparatus. First, we superglued a very thin aluminum plate to the vertical section of the right-angle arm, so that the impulse would be horizontal. Next, we mounted the apparatus on a large tripod. The base of the tripod possesses leveling feet, and has radius 9 inches. We replaced the original upright with a 6-foot long 1-inch diameter aluminum rod that is bolted onto the tripod. A hole was drilled in the drop-launch apparatus so that it could be similarly bolted to the rod. The hole was counterbored to recess the bolt head so that an inclinometer could be placed on the top of the drop-launch apparatus to level it. A photograph of the apparatus is shown in Figure 5.

Drop-launch mechanism mounted on a large modified tripod. The height of the entire apparatus is nearly 2 m.

Figure 5. Mounted Drop-Launch Mechanism.

2. Approximate Effect of Small Angle of Inclination

In experiments of the two-bullet problem, there is a relatively small time *difference* of the projected and dropped the balls striking the floor. A potential experimental problem that affects the projected ball but not the dropped ball is a small deviation of the angle of inclination of the apparatus. We quantitatively address this issue here. A positive angle of inclination of the projected ball increases the time-of-flight, while a negative angle decreases this time. We were concerned that the use of a bubble level would not be sufficiently accurate, because we are interested in the difference of the times-of-flight of

the dropped and launched balls. We thus used a digital inclinometer. A quantitative estimate of the effect of a small inclination of the apparatus is calculated below.

We let θ denote the initial angle of inclination of the projected ball, with corresponding time-of-flight T, where T_0 is the time-of-flight for $\theta = 0$. For $\theta > 0$, the time T is greater than T_0. For $\theta < 0$, T is less than T_0. Our goal here is to determine the deviation of T due to values of θ in a neighborhood of $\theta = 0$. To estimate this deviation, we neglect the effect of drag.

The vertical displacement of a projectile launched at height h with initial speed v_0 and angle of inclination θ is

$$y = h + v_0 \sin(\theta) t - \frac{1}{2} g t^2 .$$

Setting $y = 0$ and $t = T$, solving the quadratic equation for T, and rejecting the $T < 0$ solution, yields the time-of-flight

$$T = \frac{v_0}{g} \sin(\theta) + \sqrt{\frac{v_0^2}{g^2} \sin^2(\theta) + \frac{2h}{g}} .$$

To first order in θ, the squared sine term is negligible, and this expression yields

$$T(|\theta| \ll 1) = \frac{v_0}{g} \theta + \sqrt{\frac{2h}{g}} = T_0 + \frac{v_0}{g} \theta , \qquad \text{(B.1)}$$

where the time-of-flight for $\theta = 0$ is

$$T_0 = \sqrt{\frac{2h}{g}} . \qquad \text{(B.2)}$$

A dropped body has the *same* time-of-flight as a horizontally-projected body, so the time difference of the projected and dropped times is just the difference of the expressions (B.2) and (B.1):

$$\Delta T = T - T_0 = \frac{v_0}{g}\theta \ . \qquad \text{(B.3)}$$

In the experiment described in Section B.3, we used a digital inclinometer that has uncertainty $\pm 0.1^o$. For $v_0 = 5.0$ m/s and $\theta = 0.1^o = 1.75 \times 10^{-3}$ rad, the expression (B.3) for the time difference yields roughly $\Delta T = 1$ ms. This value is highly negligible for our experiment, because we are interested in a lecture demonstration with a clearly perceptible time difference of at least roughly 0.2 s. The error in the levelness of the apparatus is thus insignificant. However, a change in levelness could occur due to the handling of the apparatus during the firing and release of the balls. However, if the angle of inclination is 1^o, the time difference is only roughly 0.01 s, which is still negligible.

Also in Section B.3, we use the expression (B.3) to approximate the angle of projection that could account for the observed time difference of the projected and dropped motions.

3. Dropped and Projected Balls

To observe whether a dropped body hits the floor before a horizontally-projected body, we used the apparatus shown in Figure 5 with two Styrofoam balls of nominal diameter 1-inch (specifically, 2.34 cm; refer to Table 2). The effect was very clearly observed, with a time difference of roughly $\Delta T \approx 0.2$ s. To more precisely determine the value, we used a microphone to detect the sound due to the simultaneous release and launch of the balls, and then the balls striking the floor. The microphone output was connected to a Stanford Research Systems SR560 Preamplifier that was in turn connected to an Agilent Infinium 54810A Oscilloscope, which was triggered by the sound of the release-launch mechanism. Due to the lightness of each ball (0.22 g), however, the impact on the floor was not clearly registered on the oscilloscope. We found that large sheets of aluminum foil (18 inches by roughly 20 inches) placed in each landing area substantially increased the amplitude of the sound. But finding a location of the microphone to obtain a clear record of the three sound impulses was difficult.

We found it much easier to perform two separate sets of time measurements: one for the dropped ball and one for the projected ball. We used the same ball, and we triggered on the release-launch and measured 10 times-of-flight each for T_{proj} and T_{drop}. The two averages and their standard deviations of the mean are shown on the one-dimensional graph in Figure 6. The resultant time difference is $\Delta T = T_{proj} - T_{drop} = 0.222 \pm 0.024$ s. The error bars in the graph are due to two effects. First, there is sensitivity to the initial conditions, especially in the case of the projected ball, which is why that error bar is significantly greater. Second, we strongly suspect that there are fluctuations during the flights of the balls, due to air currents and the slight lack of roundness of the ball. The fluctuations again especially occur for the projected ball.

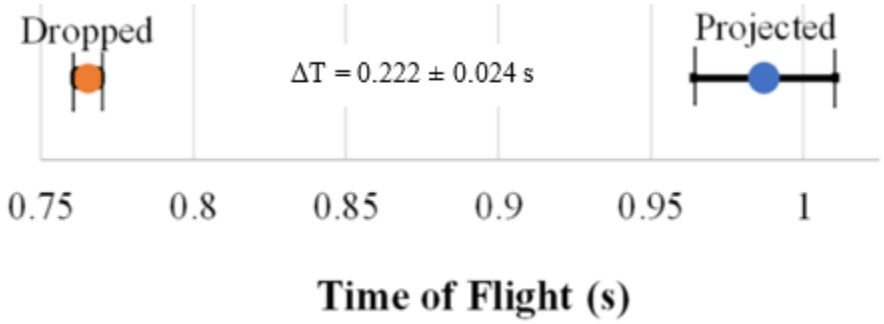

One-dimensional graph of the experimental times-of-flight for the dropped and projected motions. Ten trials were done in each case.

Figure 6. 1-D Graph of Experimental Times of Flight.

The above results include a correction due to the finiteness of the speed of sound. For the dropped motion, the microphone was placed such that there was the same distance between the drop-launch apparatus and the point of impact on the floor. There was thus no error due to the speed of sound. However, for the projected motion, the microphone was placed 1.5 m closer to the point of impact, in order to more clearly register the sound. The measured time-of-flight was thus *smaller* than the correct value by the amount of time required for the sound to travel that distance:

$$\text{time} = \frac{\text{distance}}{\text{speed of sound}} = \frac{1.5\ \text{m}}{343\ \text{m/s}} = 4.4\ \text{ms}\ ,$$

which has been added to T_{proj} in the above analysis.

The trajectory of the projected ball was observed to strongly curve outward (Figure 7). This is expected because the rotational motion of the aluminum right angle, upon which the balls initially rest at either end, undergoes rotational motion when the apparatus is fired. It is very reasonable that the rotational motion causes a horizontal counterclockwise spin of the projected ball. The Magnus effect is then responsible for the curved trajectory. The curvature is substantial. The horizontal angle between the direction of initial projection and the landing point is roughly 15^o to 20^o. In addition, the landing point substantially varies by as much as roughly 8 inches (20 cm) in any direction from the average landing point. The average range is approximately R = 2.5 m.

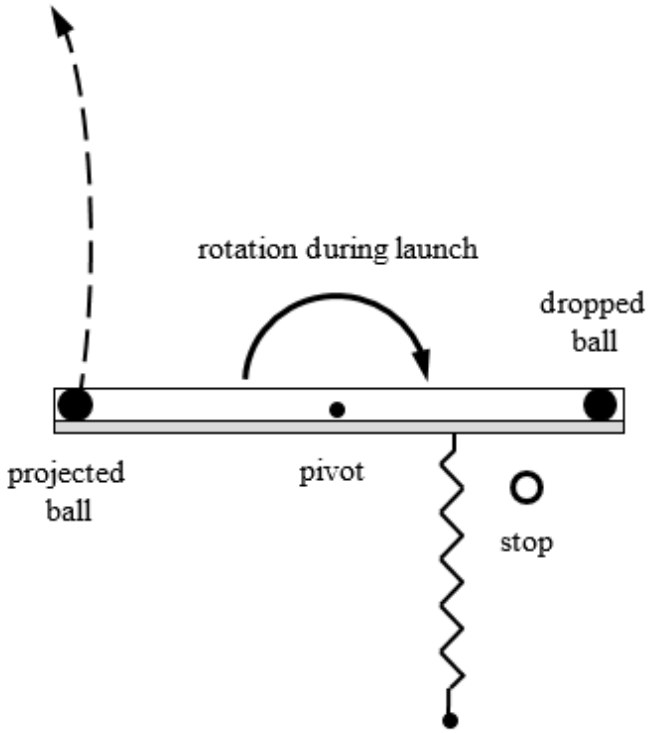

Due to the rotation of the aluminum right angle, the projected ball is given a horizontal counterclockwise spin, which causes the ball to curve outward

Figure 7. Top View of Drop-Launch Apparatus.

To compare our experimental results to computer simulations (Section 2.C), we needed to know the initial height h and projection velocity v_0. The height is measured to be h = 1.95 m. To measure the velocity, we used an older-model Daedalon photogate system, which conveniently includes an electronics box that displays the interrupted time. The system is intended for use with gliders on an air track, but we readily adapted it for our use (Figure 8). We found that the initial velocity is

$$v_0 = \frac{\text{diameter}}{\text{time}} = \frac{2.3\ \text{cm}}{3.4\ \text{ms}} = 6.8\ \frac{\text{m}}{\text{s}}\ .$$

Photogate apparatus with stop clock to measure the initial velocity v_0 of the Styrofoam ball. The diameter is divided by the maximum interrupt time.

Figure 8. Photogate Apparatus.

There is a substantial disagreement between the experimental time difference ΔT_{exp} = 0.222 s and the result of a computer simulation (Section 2.C) which predicts that the time difference is ΔT_{theo} = 0.0646 s. The experimental value is a factor of 3.4 greater than the theoretical value. In addition, the experimental range $R_{exp} \approx 2.5$ m, whereas the simulation value is R_{theo} = 2.35 m. We identified six possible sources of error that could be responsible for the discrepancy: 2 possible computer modeling problems, and 4 possible experimental artifacts. We consider each of these in turn:

1. *A purely quadratic drag does not accurately model the motion of the dropped ball and projected balls.* The Reynolds number for the projected ball is $Re = \rho v_0 D/\mu$, where

the density of air is $\rho = 1.20$ kg/m^3, the velocity is $v_0 = 6.8$ m/s, the diameter is $D = 2.34$ cm, and the shear viscosity of air is $\mu = 18.1$ μPa·s. These values yield $Re = 1.1 \times 10^4$, which is well within the flat region of the drag coefficient vs. Reynolds number for a sphere, so the drag is quadratic. The drag on the dropped ball is linear for sufficiently small times. This effect causes an increase in the drag coefficient, which increases the time-of-flight of the dropped ball and thus *decreases* the time difference $\Delta T = T_{proj} - T_{drop}$. The effect can therefore *not* account for experimental observation of an increased ΔT.

2. *In addition to the horizontal spin, the launching mechanism imparts a backward spin (bottom to top in the direction of translational motion).* This additional spin, which causes a baseball to rise, would cause the ball to remain longer in flight, and thus increase ΔT. The spin is not expected to occur. However, high-speed video of the ball, appropriately marked to show a change in orientation, could be used to determine if the spin is occurring.

3. *The ball is somehow launched with a small positive angle of inclination, even though the apparatus was carefully leveled.* This effect would cause the ball to remain in flight longer, and thus yield a positive value of ΔT. We can use Equation (B.3), which holds for no drag, to roughly estimate the positive angle of projection that would cause the observed time difference $\Delta T = 0.217$ s. The angle is roughly

$$\theta = \frac{g}{v_0}\Delta T = \frac{9.8\ \text{m/s}^2}{7.0\ \text{m/s}} \times 0.217\ \text{s} = 0.31\,\text{rad} = 17^o\ .$$

Such a significant angle would be easily detectable by eye, but was *not* observed.

4. *The horizontal spin and downward trajectory somehow cause a lift force.* We do not currently have a basis for this effect. But it would amount to a secondary Magnus force, where the primary Magnus force causes the horizontal curving shown in Figure 7. An example of how a perpendicular coupling can arise is in the motion of a rifled bullets, which curves to the left for clockwise spin along the axis. The effect is called *gyroscopic drift*.

5. *Buoyancy is not included in the calculation.* This effect is considered in Section 3.C, where we show that it causes an increase in ΔT. However, the result of a computer

simulation that includes buoyancy shows that ΔT increases by only 3.4% in our case. In addition, the range increases by only 1.1%.

6. *The porosity of the styrofoam ball causes the drag coefficient to be significantly greater that the standard value of a rough sphere, which is used in the computer simulations.* This possibility increases the drag force, and is thus expected to increase the value of ΔT. The effect of the porosity on the drag coefficient is addressed in the next section (B.4), where we show that the increase in drag due to the porosity is not sufficient to account for the value of ΔT.

In summary, it appears that the only possible above explanations for the observed value of ΔT being systematically greater than zero are #2 and #4, both of which involve spin.

4. Drag Coefficient of Styrofoam Ball

The previous experiment (Section B.3) yielded a clearly perceptible time difference of ΔT = 0.22 s of the dropped ball striking the floor before the horizontally-projected ball. However, computer simulations (Section C.1) predict a smaller time difference by a factor of more than 3. The Styrofoam ball used in the experiment is highly porous. It is reasonable that the porosity could increase the drag coefficient beyond the standard value of $C_D = 0.47$ for a sphere, perhaps to the extent that would account for the greater experimental value of the time difference. If this hypothesis is correct, however, the range according to the computer simulation should be *greater* than the observed range, but this is *not* the case: The simulation yields a range that is somewhat less. It is thus very unlikely that an increase in the drag coefficient could account for the discrepancy between the experimental and theoretical values of ΔT.

However, to directly explore the possible increase in drag, we performed an experiment to determine the drag coefficient of the Styrofoam ball. For quadratic drag, the time-of-fall from rest is given by Equation (A.8):

$$T_0(h) = \frac{1}{\sqrt{\gamma g}} \cosh^{-1}\left(e^{\gamma h}\right), \qquad \text{(B.4)}$$

where γ is the quadratic drag factor. From Equation (A.6), the terminal velocity is $v_t = (g/\gamma)^{1/2}$. In addition, from Equation (A.10), for the frontal area $A = \pi d^2/4$, we have $\gamma = \pi\rho d^2 C_D/8m$, so the value of the drag coefficient C_D can be determined from the value of γ. In fact, any of the values of γ, C_D, and v_t, can be determined from any other value.

The idea of the experiment is to plot experimental data of T_0 for different values of h, and then fit the curve in Equation (B.4) to determine γ. A potential problem is that the drag coefficient is independent of velocity only for a range of velocities. The upper limit is not a problem in our case because the velocities are very much smaller that the speed of sound. Fortunately, the lower limit turns out also to not be a problem in our case, because terminal velocity was observed to occur over a substantial range of the data, as we now show.

We adapted the acoustic method in Section 3.B to measure the time-of-flight T_0 of the dropped Styrofoam ball as a function of the height h. The apparatus is shown in Figure 9. We utilized nearly the entire 12-foot height of the laboratory to include as much, if any, of the terminal-velocity motion as possible. The microphone was always adjusted to be halfway between the drop mechanism and the floor, so that no corrections for the finite speed of sound were required. As in the previous case in Section 3.B, a large sheet of aluminum foil on the floor substantially increased the sound from the impact of the Styrofoam ball.

The drop-launch apparatus and microphone were attached to a 3/4-inch diameter aluminum rod of length 12-feet 1/8-inch, which sufficiently penetrated the acoustical ceiling tile to securely hold the rod. Meter sticks of length 2.0 and 1.0 m, with an additional length of 65 cm, were taped to a square aluminum rod that was cut to the same length as the circular rod. The side length of the square rod is approximately 3/4 inches.

Figure 9. Upper and Lower Parts of Apparatus to Determine the Drag Coefficient of a Styrofoam Ball.

Electrical and mechanical noise, especially at 60 and 120 Hz, was a problem. We reduced the noise to an acceptable level by placing a piece of rubber between the microphone and the clamp that supported it. In addition, on the SRS preamplifier, we used a high-pass 120 dB/octave filter set at 300 Hz.

A right-angle plastic triangle was used to accurately set the height of the bottom of the ball to heights with an increment of 25.0 cm, which yielded 14 data points. The data are shown in Figure 10.

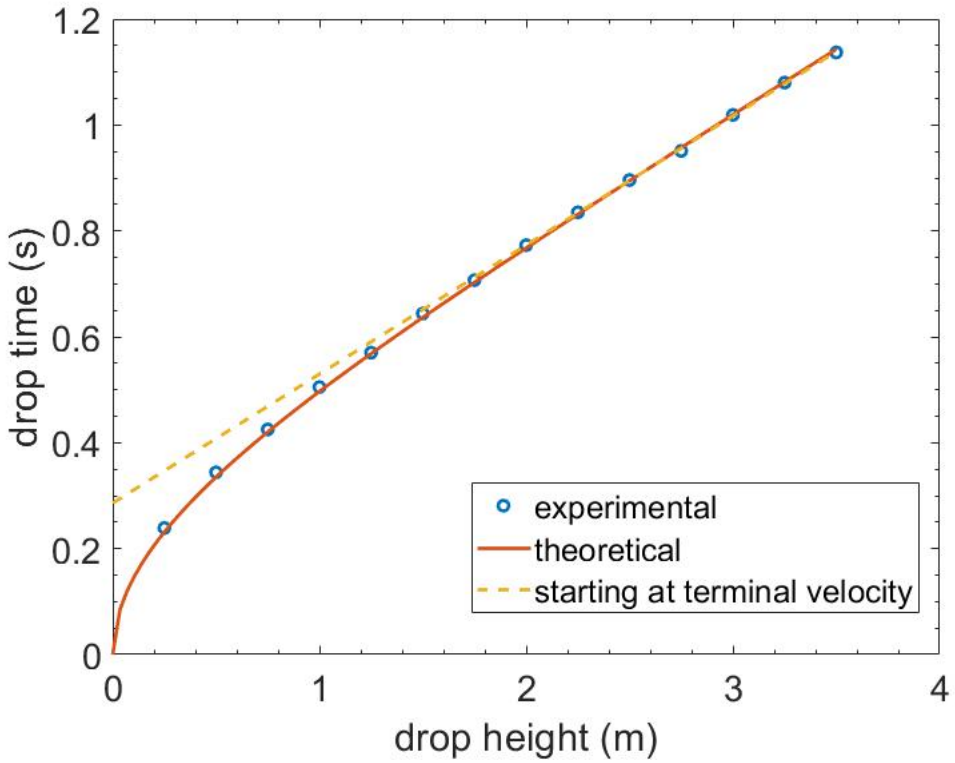

The asymptotic terminal velocity is clearly observed (dotted line). The best-fit curve corresponds to the quadratic drag theory.

Figure 10. Data from Freefall Experiment.

The value of the quadratic drag factor corresponding to the best-fit curve, as well as the corresponding values of the drag coefficient and terminal velocity are:

$$\gamma = 0.586\ \mathrm{m}^{-1}, \tag{B.5}$$

$$C_D = \frac{8m\gamma}{\pi\rho d^2} = \frac{8\times\left(0.22\times10^{-3}\right)0.586}{1.204\pi\times\left(2.34\times10^{-2}\right)^2} = 0.498, \tag{B.6}$$

$$v_t = \sqrt{\frac{g}{\gamma}} = \sqrt{\frac{9.81}{0.586}} = 4.09\ \frac{\mathrm{m}}{\mathrm{s}}. \tag{B.7}$$

We can check the value of the terminal velocity by determining an asymptotic value of $\Delta h/\Delta t$ (inverse slope of the dashed line in Figure 10). This approximately yields 4.11 m/s, which is in excellent agreement (0.5%) with the value in Equation (B.4).

The theoretical values of the parameters are $\gamma = 0.55\ \mathrm{m}^{-1}$, $C_D = 0.47$, and $v_t = 4.2$ m/s. Our observed values of γ and C_D in Equations (B.5) and (B.6) are only about 6% greater than the theoretical values, and our observed value of v_t in Equation (B.7) is only about 3% greater than the theoretical value. Furthermore, according to our computer simulations (Section C.1), the theoretical value of $\Delta T_{theo} = T_{proj} - T_{drop}$ is only increased from $\Delta T_{theo} = 0.064$ s to $\Delta T_{theo} = 0.065$ s. The range decreases from 2.35 m to 2.28 m. We conclude that the significantly-greater observed value $\Delta T_{exp} = 0.22$ s in the Section B.3 is *not* due to the porosity of the Styrofoam ball.

C. COMPUTER SIMULATIONS

1. Feasibility of Lecture Demonstration

The goal of our research of the two-bullet problem is to produce a demonstration that clearly shows the time-of-flight difference $\Delta T = T_{proj} - T_{drop}$ of two identical bodies, where one is simultaneously dropped from rest and the other is horizontally projected, both at the same initial height. Because the equations of motion are coupled and nonlinear in the projected case, we cannot analytically solve for ΔT. We therefore utilize computer simulations. The goal of these is to pinpoint parameters that optimize ΔT. From there, the

goal is to find a region of parameters with which we could produce a classroom demonstration apparatus.

The simulation utilizes Euler's method to approximate the horizontal and vertical motion of the trajectories:

$$x(t+\Delta t) = x(t) + v_x(t)\Delta t$$

$$y(t+\Delta t) = y(t) + v_y(t)\Delta t .$$

The instantaneous velocity components are calculated from the acceleration components, also by Euler's method:

$$v_x(t+\Delta t) = v_x(t) + a_x(t)\Delta t$$

$$v_y(t+\Delta t) = v_y(t) + a_y(t)\Delta t ,$$

where the instantaneous acceleration components are

$$a_x(t) = -\gamma v(t) v_x(t)$$

$$a_y(t) = -\gamma v(t) v_y(t) - g . \qquad \text{(C.1)}$$

In the last two expressions, the magnitude of the velocity is

$$v(t) = \sqrt{v_x^2(t) + v_y^2(t)} .$$

This simple classic algorithm is a first-order method wherein the error is proportional to the square of the step size; therefore it is an acceptable approximation for sufficiently small increments of Δt. The full computer program is in App. A. We checked the program for the time-of-fall in the dropped case, which has the analytical solution (A.8).

Keeports (1997) employed the same numerical method, and used the time step Δt = 2.0 ms. We confirmed that our program yields identical results for that time step. For our investigations, we use the smaller time step Δt = 1.0 μs for better accuracy.

We began the simulations by assuming that a larger quadratic drag coefficient γ would result in larger time difference ΔT between the launched and dropped cases. After all, without the quadratic drag, the two projectiles would hit at the same time (Section A). But we soon discovered that ΔT does *not* monotonically increase with increasing γ. Surprisingly, for any fixed initial velocity v_0 and height h, there is a value of γ that *maximizes* ΔT. The top graph of Figure 11 shows ΔT as a function of γ for different values of v_0 and for a fixed initial height of h = 2.0 m. The bottom graph is the corresponding horizontal range R of the projected body also as a function of γ, for the same values of v_0 and h.

For a qualitative lecture demonstration, the minimum clearly perceptible difference of the time-of-flight ΔT is approximately 0.2 s. We arrived at this criterion independently of Keeports (1997), who states the same value. The top graph of Figure 11 shows that this is only possible for an initial velocity of roughly 100 m/s, which is impractical for a lecture demonstration. We conclude that, as we have envisioned it, *a lecture demonstration showing that a dropped body strikes the floor before a horizontally-projected body is not feasible!*

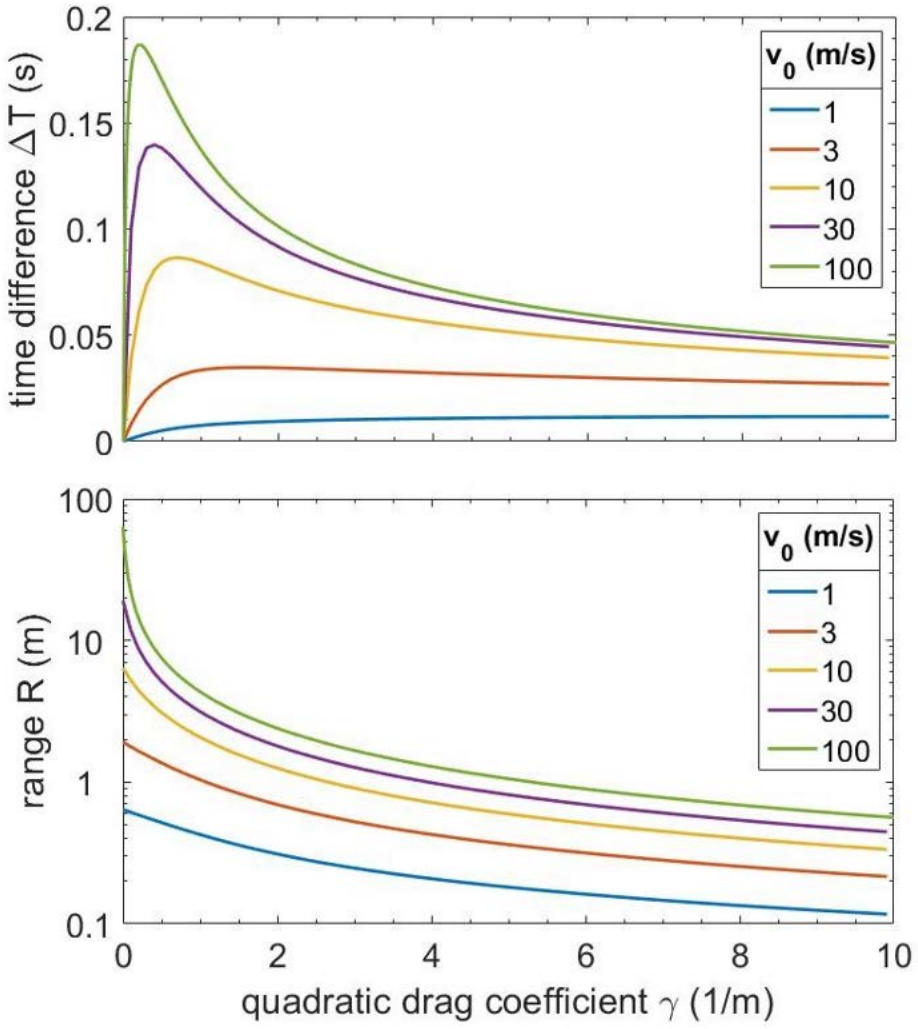

The initial height is h = 2.0 m.

Figure 11. Time Difference (Top) and Range (Bottom) versus Quadratic Drag Coefficient for Various Initial Velocities.

To understand why there is a maximum value of ΔT as a function of γ in the top graph of Figure 11, first note that we must have ΔT = 0 for $v_0 = 0$. because the motions of the projected and dropped bodies are identical in this case. Next, we consider the most dramatic case which occurs for the initial velocity v_0 = 100.0 m/s, yielding a maximum value of ΔT at approximately γ_{max} = 0.2 1/m. In general for quadratic drag, the horizontal motion of a launched projectile exponentially approaches a vertical asymptote of maximum

range (provided the projectile does not strike the ground). This phenomenon is discussed by Taylor (2005), and can be seen in Figure 12 for several successive values of γ. A vertical asymptote cannot be analytically determined. The asymptotes in the graph were determined numerically by extending the motion to sufficiently negative values of the vertical coordinate. As seen in the bottom graph of Figure 11, an increase of γ in a neighborhood of γ_{max} causes a substantial decrease in the range. The projected body relatively quickly approaches the motion of a dropped body, and this effect increases as γ is increased. This motion *reduces* the time difference ΔT, so a maximum value is expected.

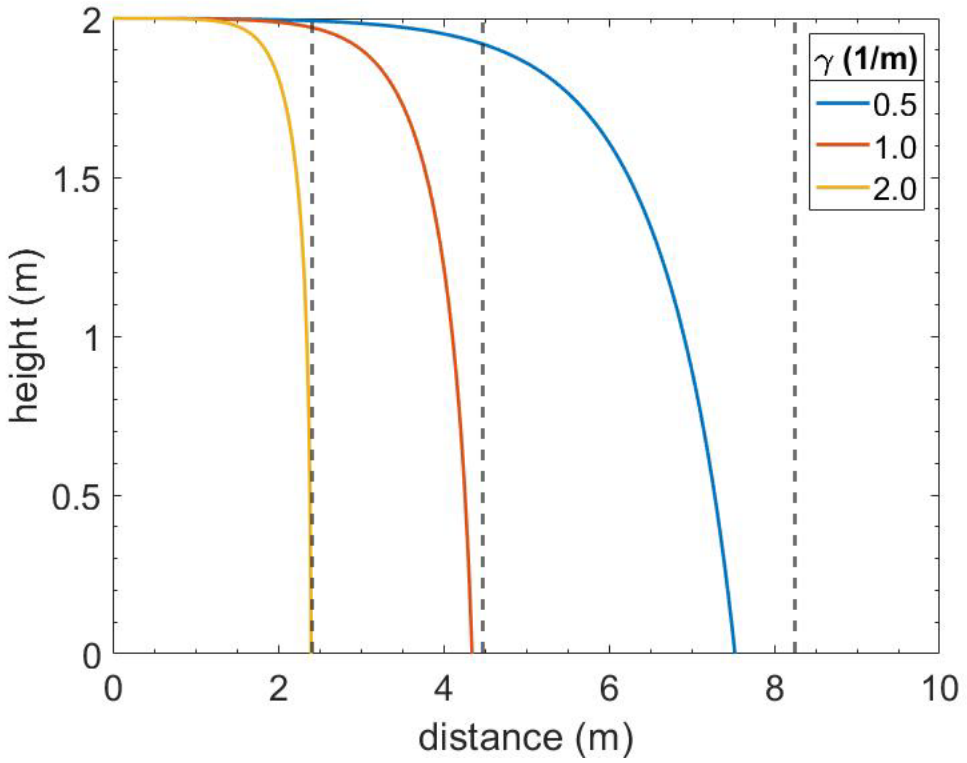

The initial velocity is v_0 = 100.0 m/s, and the quadratic drag coefficient is γ = 0.5, 1.0, and 2.0 1/m. Quadratic drag causes the horizontal motion to exponentially approach a vertical asymptote.

Figure 12. Projectile Simulation Results for No Drag and for Quadratic Drag.

2. Bullets

An episode of the popular MythBusters television show covered the two-bullet problem. An experiment was conducted by firing an actual gun horizontally while the apparatus simultaneously dropped another bullet, with both bullets at the same initial height. A high-speed camera was used to measure the difference in times-of-flight. The measured time difference was ΔT = 39.6 ms, and the range was roughly R = 110 m. MythBusters considered such a small value of ΔT to be due to experimental errors, and that the result of the experiment was therefore that both bullets struck the floor at the same time within experimental error. It was not stated which bullet hit the floor first, but an examination of a slow-motion video in the show reveals that the dropped bullet struck the floor first.

The type of bullet used by MythBusters was not specified. We assume a .45 caliber bullet because this is a heavier bullet with greater drag, and velocities not approaching the speed of sound in air. The parameters are: mass m = 15 g, diameter d = 1.15 cm, drag coefficient C_D = 0.295, and initial velocity v_0 = 255 m/s. The Reynolds number is approximately Re = 2 x 10^5, which puts the motion in the regime of quadratic drag.

According to our simulations, for an initial firing height of 1.0 m, a .45 caliber bullet yields a theoretical time difference of ΔT = 10.2 ms and a range of R = 110 m. Considering this was a guess of what type of gun they used and we were not physically present during the experiment, it is difficult to pinpoint exact sources of error between this theoretical time difference and the MythBusters experimental value. However, the MythBusters measured time difference of 39.6 ms is within a factor of 4 of the simulation value, and the imprecise range provided by MythBusters is the same as the simulation. This indicates that the measurement of the time difference is not completely a result of experimental error, but is partly due to the quadratic drag on the fired and dropped bullets.

3. Inclusion of Buoyancy

Motivated by the results of Keeports (1997), and because we wondered if the buoyant force due to the air could have played a role in causing the dropped ball to clearly strike the floor before the projected ball (Section B), we now generalize the time difference

$\Delta T = T_{proj} - T_{drop}$ to include buoyancy acting on the projected and dropped bodies. Buoyancy is a constant force that acts only in the vertical direction opposite to gravity. We consider the case in which the body is denser than air. The existence of buoyancy in the system is equivalent to deceasing the acceleration of gravity; that is, the effective gravitational acceleration g_{eff} is less than g. This smaller downward acceleration increases the times-of-flight for both the projected and dropped cases. Because g_{eff} enters linearly in the equations that describe the motions of the two bodies, it is natural to guess that the two times-of-flight increase by the *same* amount, so the time difference ΔT remains the same. However, computer simulations show that the increase of T_{proj} is greater than the increase of T_{drop}, so ΔT *increases*.

To understand why buoyancy increases the difference of the times-of-flight, we consider the vertical equations of motion of the dropped and projected bodies. The net vertical forces per unit mass on the bodies are

$$f_{drop} = g - \gamma v_y^2 \quad \text{and} \quad f_{proj} = g - \gamma v_y \sqrt{v_x^2 + v_y^2},$$

where the positive direction is taken to be downward, and where g is understood to be the effective gravitational acceleration. Decreasing g does not appear to change the difference of the forces. But this assumes that v_x does not change, which is not valid due to the coupling between the x and y motions. In the limiting case where gravity dominates the drag, the time difference $\Delta T = T_{proj} - T_{drop}$ vanishes. When the quadratic drag is not negligible, we know that $\Delta T > 0$ (Section A.3). By decreasing the value of g, we are increasing the role played by the drag, so it is reasonable that ΔT increases. This is only a plausibility argument, but it is all that we currently have. A rigorous argument is left for future work.

To quantify the effect of the buoyancy, we begin with Archimedes' law, which states that the buoyant force B is the weight of the displaced fluid:

$$B = \rho V g,$$

where V is the volume of the body, ρ is the density of fluid (in our case, air at room temperature and atmospheric pressure), and g is the acceleration due to gravity. The net vertical force due to the gravitational and buoyant forces is F = mg – B. Because B is proportional to g, we can conveniently express the net force as F = mg_{eff}, where the effective acceleration due to gravity, which includes buoyancy, is

$$g_{eff} = g - \frac{B}{m} = g\left(1 - \frac{\rho V}{m}\right) = g\left[1 - \frac{4}{3}\pi\left(\frac{d}{2}\right)^3 \frac{\rho}{m}\right].$$

In the final step, we have assumed a spherical body of diameter d. Buoyancy is included in the computer program by simply replacing g with g_{eff}. The fractional reduction of g_{eff} from g is

$$\frac{g - g_{eff}}{g} = \frac{4}{3}\pi\left(\frac{d}{2}\right)^3 \frac{\rho}{m}.$$

Substitution of the values for our Styrofoam ball yields

$$\frac{g - g_{eff}}{g} = \frac{4}{3}\pi\left(\frac{2.34 \times 10^{-2}}{2}\right)^3 \frac{1.20}{0.22 \times 10^{-3}} = 3.7\%, \qquad \text{(C.2)}$$

which is expected to have only a small effect on the time difference. This is indeed the case: Computer simulations with g_{eff} for our experimental initial conditions of h = 1.95 m and v_0 = 6.8 m/s yield ΔT = 0.0668 s. For g instead of g_{eff}, we find ΔT = 0.0646 s. The increase of ΔT for g_{eff} is only 3.4%, which is approximately the same as the deviation (C.2). The range increases from R = 2.322 m to R = 2.349 m, which is an increase of only 1.2%.

According the results of Keeports (1997), which we quantitatively verified with our computer code, the decrease in the effective acceleration due to gravity acts to significantly increase the value of ΔT when g_{eff} is substantially less than g, which occurs when the average density of a body is a relatively small amount greater than the density of the fluid.

D. CONCLUSIONS AND FUTURE WORK

Lecture demonstrations of the two-bullet problem are common, but the drag is negligible in these cases. The dropped and horizontally-launched bodies strike the floor with an imperceptible time difference, which occurs due to the near absence of coupling of the horizontal and vertical motions. When the effect of drag is considered, the problem becomes more interesting. Linear drag does not introduce a time difference, because the horizontal and vertical equations of motion remain uncoupled. Constant drag causes the projected body to strike before the dropped body, while the common case of quadratic drag causes the opposite to occur. In this chapter, we investigated the possibility of a lecture demonstration of the quadratic drag case.

Experiments with a commercial apparatus showed that a launched Styrofoam ball clearly strikes the floor before a dropped ball, but computer simulations showed that the time difference for a model system is substantially less. Further experiments ruled out a number of possible artifacts except those related to the spin that the apparatus imparts to the projected ball. The computer simulations reveal that perceptible time differences for practical lecture demonstration apparatuses do not occur. The reason is that the launched projectile exponentially approaches a maximum range due to quadratic drag, and that this range is small for practical parameters. The result is that the time difference has a maximum value as the quadratic drag coefficient is increased, and that this value is imperceptibly small for practical lecture demonstrations. Actual fired and dropped bullets were used in an episode of the MythBusters television show. However, the show incorrectly attributes all of the small measured time difference to experimental error rather than quadratic drag.

As discovered by Keeports (1997), an exception of very small time differences occurs when the acceleration due to gravity is sufficiently small, which can be effectively achieved due to buoyancy acting on the bodies. However, simulations show that the effect is too small to explain the time difference of the Styrofoam balls in our experiments. For a perceptible time difference to occur, the bodies must have an average density that is only slightly greater than that of air, and this is not practical for a convincing and convenient lecture demonstration.

There is a variety of possible future work related to demonstrations of the two-bullet problem. One possibility is to experimentally confirm the imperceptible time difference for the Styrofoam balls. In an initial attempt, we removed the problem of the 3B Scientific apparatus imparting a spin to the Styrofoam ball by modifying the Pasco apparatus to have a slender pin attached to the drop end side of the rod with a hollow cylinder attached to the frame on the drop side. The length of the cylinder is equal to the length of the pin so that the pin is completely within the cylinder when the apparatus is unarmed, but the pin sticks out when armed. The Styrofoam ball can then be attached to the apparatus by inserting the ball into the pin. The ball would then drop when the apparatus is fired. However, the apparatus still experienced complications. For the dropped case, some projection occurs due to the Styrofoam ball moving back when fired and bouncing off the cylinder. Also, the projected ball has an unwanted vertical component, likely due to the apparatus striking it off center. The apparatus would be improved by slightly sanding the rubber base on the projected side so that the rod hits the Styrofoam ball directly in the center when fired. Alternatively, a flat surface can be applied to the rod on the projected side. In addition, the pin on the drop side needs to be reattached with more permanent glue, along with the cylinder. The pin and cylinder both also need to be adjusted so that the Styrofoam ball does not bound against the cylinder when the apparatus is fired. This could likely be achieved by shortening the pin and cylinder.

A different perspective of possible future work is to understand why the 3B Scientific apparatus yields a perceptible time difference, which is apparently due to the spin. There are two possibilities here. First, the apparatus may be imparting a spin about the horizontal axis perpendicular to the initial velocity such that the ball experiences an upward force (a “riser” in baseball). This effect would cause an increase in the time difference ΔT. High-speed video of a Styrofoam ball with markings could show if the apparatus is imparting this spin. Second, due to rotating arm that launches the ball, there is a substantial spin about the vertical axis which causes the ball to curve substantially outward from the apparatus, due to the Magnus force. In combination with the downward trajectory, it is conceivable that this spin may produce a secondary Magnus force about the horizontal axis perpendicular to the velocity. This effect, if it exists, would be of

fundamental importance in fluid mechanics. Simulations with computational fluid dynamics software could be done to observe whether the effect occurs.

There are also two possibilities of future work that involve the fact that buoyancy increases the time difference ΔT between the dropped and projected balls striking the floor. First, it is not physically clear why this effect occurs. We presented only a plausible argument; a rigorous explanation is needed. Second, there needs to be a two-dimensional color graph that reveals mass and diameter values of a projectile that yield an acceptable time difference ΔT. The mass m could be labeled on the x-axis and diameter d on the y-axis, where color signifies ΔT for fixed values of the height h and initial velocity v_0. A standard color spectrum could be used to denote values of ΔT. The graph should include level curves for different values of g_{eff}/g. From the graph, it would be interesting to determine if there are any known planets or moons that meet the ideal g_{eff}/g ratio where the apparatus would exhibit a perceptible time difference for a Styrofoam ball. Because a reduced g corresponds to a reduced atmosphere, and thus a reduced drag, there may be *no* such planets or moons!

To obtain an apparatus that yields a clearly perceptible time difference, a possibility is to use a table-top aquarium. A small drop-launch apparatus would have to be constructed. First, however, the quadratic regime of the drag would have to be checked, because the drag may be linear in this case, and computer simulations should be done. Note that, in contrast to air, buoyancy can be readily utilized in the case of water.

III. PARAMETRIC EXCITATION OF U-TUBE OSCILLATIONS

A. BACKGROUND AND MOTIVATION

Parametric excitation is a general phenomenon where the motion of an oscillator is produced and maintained by modulating a parameter upon which the natural frequency depends (B. C. Denardo, 2017; Landau & Lifshitz, 1976). The standard example is a simple pendulum, which has natural frequency $f_0 = (1/2\pi)(g/L)^{1/2}$, where L is the length of the pendulum and g is the acceleration due to gravity. Parametric excitation can occur when either L or g is modulated (Figure 13).

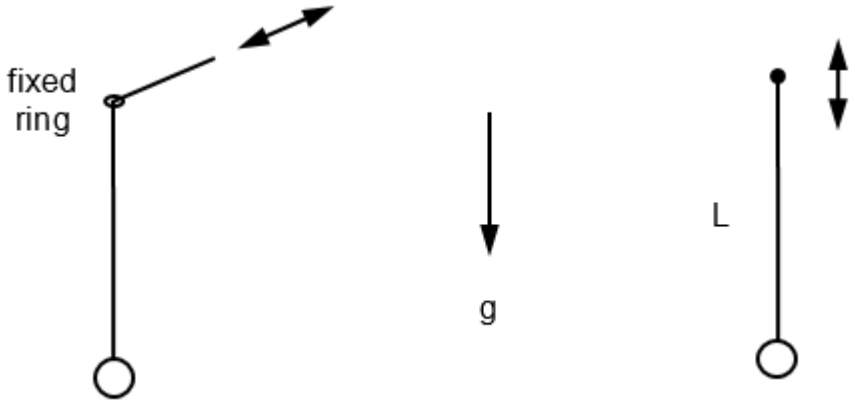

On the left, the length of the pendulum is modulated. On the right, the acceleration due to gravity is modulated in the frame of reference of the support of the pendulum.

Figure 13. Parametric Excitation of a Simple Pendulum.

Optimum parametric resonance occurs when the drive frequency is in a neighborhood of *twice* the natural frequency. In contrast to the standard case of a direct drive, parametric excitation only occurs only for drive amplitudes greater than a threshold value. The threshold is a minimum when the drive frequency is equal to twice the natural frequency. Also in contrast to a direct drive, the response amplitude grows exponentially, and is only limited by nonlinearity.

Parametric excitation has caused substantial damage to ships at sea (Neves & Rodríguez, 2007). Waves can cause a ship to vertically oscillate. If the frequency is near

twice the side-to-side rolling frequency of the ship, the vertical oscillations can parametrically excite the rolling mode. Because another mode of the system is acting as the drive here, the phenomenon is referred to as a *parametric instability*. Such an instability occurs for the in-phase normal mode of two coupled pendulums (B. Denardo et al., 1999).

A standard U-tube consists of a liquid in a tube with the shape of an upright U in a downward gravitational field. U-tubes are used as manometers (to measure pressure), and are also used on ships to damp rocking motion. The liquid in a U-tube can undergo oscillations, similar to a pendulum. However, there is a distinction between the two systems: U-tubes should be *linear* (Hooke's law holds) until the ends of the liquid enter the rounded region of the U, whereas pendulums are always *nonlinear* except in the limit of an infinitesimal amplitude. An interesting demonstration would then be to parametrically drive a U-tube just above threshold. The amplitude of the liquid should then grow, at first very slowly, but later more and more quickly, until the ends of the liquid encounter the rounded region of the U, where a nonlinearity would saturate the growth. This would be a dramatic confirmation of the relatively large amplitudes that can be obtained with parametric excitation.

Our goal is to parametrically excite and maintain U-tube oscillations by vertical displacement (Figure 14). A literature search uncovered several papers on U-tube oscillations (Donnelly & Penrose, 1956; Gilson & Boedtker, 1969; Morinigo, 1972), but no report of parametrically driven oscillations. We did find a report of parametric stabilization of inverted U-tube (Michaelis & Woodward, 1991), which is similar to that of an inverted pendulum. One of our motivations is to extend demonstrations beyond pendulums, to show the generality of parametric excitation. Another motivation is to directly show that only a nonlinearity limits the growth, which cannot convincingly be done with pendulums.

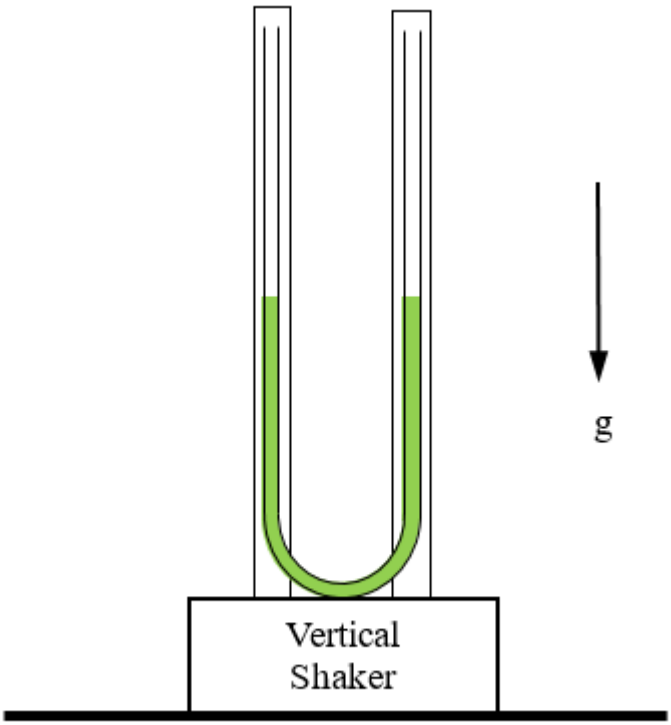

In the frame of reference of the U-tube, the vertical motion of the shaker effectively causes a modulation of the acceleration due to gravity. This modulation can theoretically excite and maintain oscillations of the liquid.

Figure 14. Parametrically Driven Liquid in a U-tube.

In Section B, we describe a transducer that we use to measure the drive amplitude of a shaker. We also present investigations of the adaptation of a subwoofer as a shaker, and we describe our U-tube apparatus. In Section C, we present U-tube free decay data which surprisingly show that the dissipation is piecewise-linear. In Section D, we present drive amplitude threshold data for parametric excitation from rest and for maintenance of steady-state oscillations. A second surprising observation is that the nonlinearity that limits the growth in our case appears to be neither due to nonlinear dissipation nor a breakdown of Hooke's law. Conclusions and future work are discussed in Section E.

B. APPARATUS

1. Linear Variable Differential Transformer (LVDT)

In our U-tube experiments, we require measurements of the displacement amplitude of the shaker. Specifically, we require the Fourier component at the drive frequency, which is the relevant drive amplitude for the parametric resonance at half that frequency. The displacements of the shaker in our case are sufficiently large that nonlinearity occurs (Hooke's law breaks down), which produces significant harmonics. We accomplish the measurements with an LVDT (linear variable differential transformer, also known as a linear variable displacement transducer).

Previous research projects utilized 1 inch peak-to-peak LVDTs, but our measurements require at least twice that range. We searched the market, and found acceptable models from 6 companies. We considered models that do *not* have built-in electronics; for greater control and accuracy, we want to use our own lock-in amplifier to demodulate the ac response. The pricing was all roughly comparable at $350, and we eventually settled on the company that seemed competent and could ship immediately: U.S. distributor RDP Electrosense, Pottstown, PA, model ACT1000, ±25 mm maximum displacement.

Our first task was to verify the factory calibration (or sensitivity). Based on the information in the specification sheet, we calculated the sensitivity be 0.333 V/cm for the operating frequency 5.0 kHz and drive voltage 1.0 V_{rms}. We use a Stanford Research Systems SR850 Lock-In Amplifier. We statically calibrated the LVDT with a Mitutoyo 50 mm peak-to-peak dial indicator with increments of 10 μm. The indicator is in vertical contact with the surface of a lab jack. A voltage reading is taken after each 2.0 mm increment of the lab jack with the knob being carefully turned by hand. The data are shown in Figure 15. The sensitivity (slope of the line) is 2.78 V/cm, which significantly disagrees with the 10X-scaled factory sensitivity of 3.33 V/cm. The factor value is incorrectly greater by 20%. We were very glad that we calibrated the LVDT! To be absolutely certain that we were not making a mistake, we approximately checked the calibration to about 3% by

taking video of the indicator while it was attached to our shaker (Section B.3). This was accomplished at a frequency of 0.5 Hz and a peak-to-peak displacement amplitude of 15 mm.

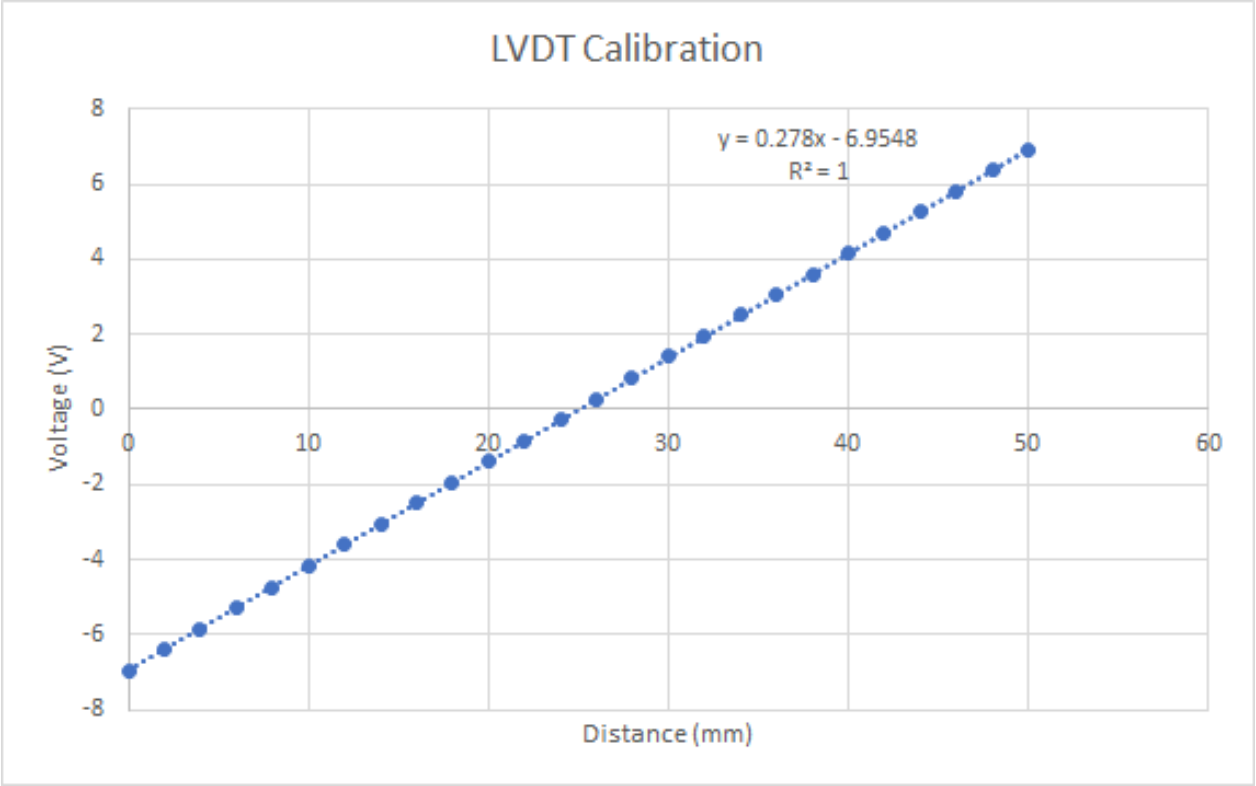

A dial indicator on a lab jack is used to statically measure the displacement as the height of the jack is varied. The indicator has the same response range as the LVDT, which is 50 mm peak-to-peak. The response is highly linear.

Figure 15. Calibration Graph for the LVDT.

We use the following lock-in amplifier settings to gather drive displacement data: 5.0 kHz, 1.0 V_{rms}, 3.0 ms time constant, and in-phase output X (rather than magnitude R, but the two are close to each other). The output of lock-in amplifier is fed to both an Agilent Infinium Oscilloscope, so that we can monitor the actual time series, and a Stanford Research Systems SR785 Signal Analyzer, so that we can measure the amplitude of the displacement at the frequency of the drive.

2. Selection of Subwoofer

A quick preliminary attempt to achieve parametric excitation of U-tube oscillations failed, which was evidently due to the maximum displacement amplitude being below threshold. We used an Acoustic Power Systems model 120S shaker with its dedicated amplifier, which delivered a maximum peak displacement amplitude of 2.1 mm before automatically shutting off. We excited U-tube oscillations by momentarily blowing into one end, and clearly observed that the motion decayed more slowly compared to no drive. This was encouraging because, as a parametric drive amplitude is increased but remains below threshold, the effective quality factor Q increases. (Threshold corresponds to infinite Q.) However, because the increase in Q was only moderate, we suspected that substantially greater drive amplitudes would be required.

We decided to consider the use of a *subwoofer*, which is a low-frequency high-amplitude loudspeaker. The common maximum peak-to-peak excursion is 2 inches. Various models of subwoofers had been previously obtained for use in nonlinear acoustics experiments in our laboratory. We gathered relevant specifications on these drivers and proceeded to test them with the LVDT (Section B.1). We drove each subwoofer at frequency 2.0 Hz with an HP 33120A function generator connected to a Techron 5530 power amplifier. The results are shown on the next page in Table 3.

We quickly narrowed the search to three subwoofers: Audio Pulse EPD212, TC Sounds 707B, and RE Audio MX-12. The deciding factor turned out to involve the power amplifier (Techron 5530). Of several amplifiers, the Techron was the one that delivered the greatest voltage of 32.5 V_{rms} into a bridged 4 Ω load. We ended up having to use the one Techron 5530 that had extra heat sinks, because our original one occasionally shut off due to high temperature. Of the three subwoofers, the TC Sounds produced the greatest displacement amplitude when driven at the maximum voltage of 32.5 V_{rms}. This is due in part to its BL factor (product of the magnetic field and the length of the voice coil). The strong magnetic field is indicated by the heavy weight (60 lbs) of the subwoofer.

Table 3. Various Low Frequency Loudspeakers Tested for Use as Parametric Drive of U-Tube

Specifications and Test Results for Various Subwoofers

manufacturer, model number, and diameter	dc resis-tance R	max peak excursion Xmax	max continuous power P and rms voltage $V_{max} = (PR)^{1/2}$	rms voltage at half-max power $V_{max}/2^{1/2}$	comments
Electrovoice EVX-155 15-inch	5.1 Ω	25 mm (0.98 inch)	1000 W 71 V_{rms}	50 V_{rms}	Substantial distortion; Smoothed square wave. Roughly 1-3/4 inch p-p.
Audio Pulse EPD212 12-inch	3.7 Ω	2.2 cm (0.87 inch)	600 W 47 V_{rms}	33 V_{rms}	Large distortion, but with only moderate harmonic amplitudes. Roughly 1-1/2 inch p-p.
TC Sounds 707B 12-inch	3.7 Ω	1.0 inch	1000 W 62 V_{rms}	44 V_{rms}	Very heavy. Smoothed square wave. Greatest displacement amplitude for fixed voltage.
RE Audio MX-12 12-inch	4.1 Ω	2.2 cm (0.87 inch)	1700 W 83 V_{rms}	59 V_{rms}	Very hot voice coil. Low distortion. Roughly 1-1/2 inch p-p.
Velodyne HGS-X 10-inch	3.4 Ω	1.0 inch	1250 W 65 V_{rms}	46 V_{rms}	Unsuitable for vertical orientation.
Audio Pulse Epic 10 DVC 10-inch	3.9 Ω	1.0 inch	600 W 48 V_{rms}	34 V_{rms}	Unsuitable due to damaged surround.

The specifications and results are stated. The TC Sound driver was eventually chosen.

In the future, an LVDT with a greater maximum displacement amplitude should be used, because this was one of the limitations of driving at higher amplitudes. Going along with this, higher amplitudes can be achieved with a low-frequency displacement drive that converts circular motion of a dc motor into rectilinear oscillatory motion. The conversion of rotational to rectilinear motion has another advantage. The distortion of this drive can be made to be negligible, which obviates the use of the signal analyzer (Section B.1). This is desirable for the following reason. Due to the low drive frequency (approximately 2.0 Hz), and our desire to take threshold data at small frequency differences (Section D), the acquisition time is long (32 s). During this time, changes can occur in the system. For example, the temperature of the voice coil of the shaker (Section B.2) can increase, which reduces the drive amplitude for a fixed frequency. However, it should be noted that it would

be tedious to change the drive amplitude for the dc motor system, and we are required to do this often while taking threshold data.

3. Construction of U-Tube Apparatus

The flow of the liquid in a U-tube is often substantially dissipative; that is, the quality factor Q is low. The threshold drive amplitude for parametric excitation is inversely proportional to Q (Section D.1), so it may be difficult to achieve a drive amplitude that is greater than the threshold value; that is, parametric excitation may *not* be possible. One remedy may be to use a U-tube of greater diameter. The reason is that, for a fixed length of the liquid and thus a fixed frequency, the drag force is proportional to the inner circumference of the tube, but the inertia is proportional to the area, so Q is proportional to the diameter. However, increasing the diameter increases the overall mass and thus lowers the maximum displacement of the driver. We decided just to try a U-tube that would be sufficiently large to be appropriate for a demonstration in a large lecture room.

First, however, we had to convert the subwoofer (Section B.2) into a shaker. To do this, we began with a 3/8-inch thick disk of expanded PVC, which has a substantially smaller density than standard PVC. The outer diameter was machined to 8.75 inch, which allows the disk to fit snugly between the surround and cone of the subwoofer. An inner diameter of 2.0 inches had to be machined to allow space for the protruding dome of the subwoofer. Holes were drilled and tapped in the disk so that the LVDT rod and the uprights that support the U-tube could be attached (see below). The disk is attached to the subwoofer with 16 segments of 3/8 x 1.25 inch lengths of machinist's double-sided tape (3M VHB), which fortunately turned out to be sufficiently strong for our range of drive amplitudes and frequencies.

For the U-tube, we used clear flexible Tygon tubing with inner diameter 0.50 inch and wall thickness 0.10 inch. The length of the tube is approximately 110 cm. The entire assembly is shown in Figure 16.

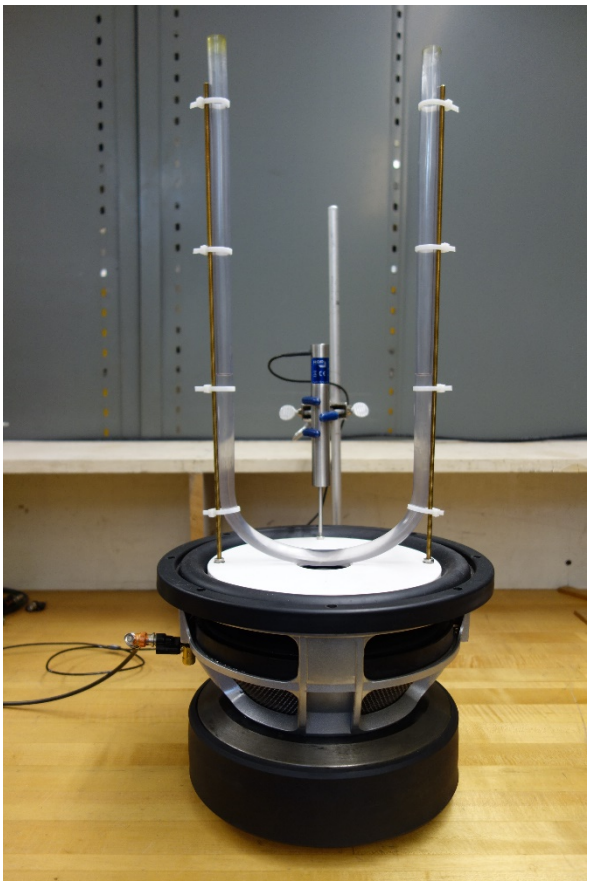

Clear flexible tubing is bent and held in the shape of a U, where the left and right arms are vertical over as a large a distance as practical, for the purpose of linear oscillations (Hooke's law). A subwoofer is adapted as a vertical shaker, and an LVDT is used to measure the displacement of the drive. The liquid is ethyl alcohol. For lecture demonstration purposes, a small amount of fluorescein is added so that the liquid can be clearly observed. For scale, the outer diameter of the subwoofer is 12.6 inches.

Figure 16. Parametrically Driven U-tube Apparatus.

The uprights are 10–32 threaded brass rods of length 18 inches. The horizontal distance between the centers of the vertical arms is 19.0 cm. Cable ties are used to attach tubing to the uprights. Attention was paid to maximize the height of the vertical arms, so that the linear (Hooke's law) regime was as large as conveniently possible. The vertical portion of arms (not including rounded sections) have length 41 cm.

The liquid in the tube has length 47.1 cm, which corresponds to the bottom of the meniscus in the right arm of the U-tube being 1.0 cm above the top of the nearest cable tie.

A precisely repeatable length is important because our drive amplitude threshold results are sensitive to the natural frequency of the U-tube oscillations (Section 3.D).

The subwoofer is driven by a function generator through a power amplifier (Section B.2). The drive displacement amplitude is measured with the LVDT (Section B.1), which is held by a clamp that is attached to the vertical rod of a tripod. A hole had to be drilled and tapped for LVDT rod because, at higher amplitudes, the rod would depart from the surface if only resting on it. The departure was not due to the acceleration exceeding g but, rather, to small amount of static friction between rod and casing. Ethyl alcohol or water with a small amount of a surfactant can be used in the U-tube. We chose the alcohol because its high vapor pressure naturally wets the wall of the tube which highly reduces pinning of the liquid on the wall. For the liquid to be clearly seen for lecture demonstration purposes, a very small amount of the strong dye fluorescein is added. This dye is used in air-sea rescue operations. We did not use the dye in our experiments because it could have possibly altered the results.

C. FREE-DECAY MEASUREMENTS

One of the goals in our research on a parametrically driven U-tube is to measure the drive amplitude threshold from rest, and to compare the data to the theoretical expression (3.5) in Section D. This expression depends upon the damping parameter β of the oscillations of the liquid, where the amplitude of a free decay in time t is proportional to $e^{-\beta t}$. A theoretical expression for β can be derived. For accuracy, however, we decided to determine β from free-decay measurements of our particular U-tube.

We recorded the period and amplitude of 11 complete oscillations. We achieved this by setting a camera 1 meter from the equilibrium point of the U-tube and attaching a ruler along one arm of the U-tube. The camera was placed away from the U-tube in order to reduce parallax error. The camera for our experiments was an iPhone 11 Pro, which was mounted on a tripod. The camera was focused and zoomed in such that the readings from the meniscus were clear to a fraction of a millimeter. To obtain accurate results, we paid attention to lighting, placement of the ruler, and reducing parallax error. We used a food baster inserted into one arm of the U-tube to create a pressure differential that brings the

liquid to a substantial amplitude before the nonlinearity due to the curved section. The baster was then removed and the camera recorded the oscillations of the liquid after a half cycle so that the wall of the tube was wetted.

From the readings, the displacement amplitude was recorded in fractions of a millimeter, and the time of the amplitudes in milliseconds. A semilogarithmic plot of the amplitude vs. time is shown in Figure 17.

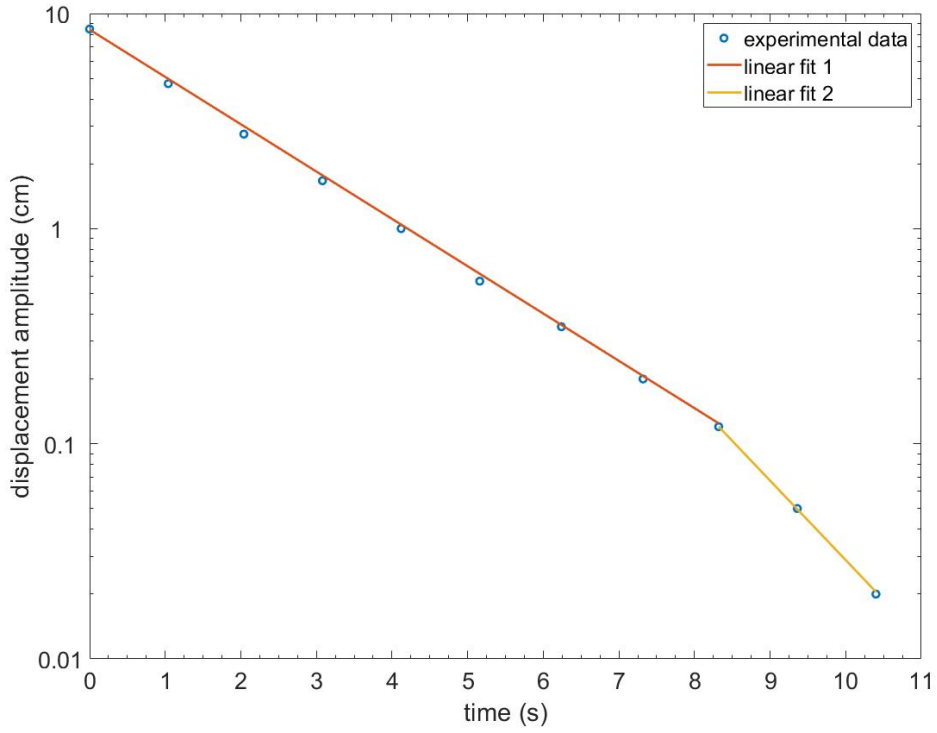

The displacement amplitudes were measured from a video recording. For the amplitude in units of centimeters, and for the time t in seconds, linear fit 1 has amplitude 8.418 exp(–0.5065 t), and linear fit 2 has amplitude 141.8 exp(–0.8502 t).

Figure 17. Semilogarithmic Plot of Free Decay Amplitude Data of U-tube Oscillations

The data surprisingly show a piecewise-linear behavior, with an upper regime of points 1–9 and a lower regime of points 9–11. These regimes respectively correspond to the damping parameter values $\beta = 0.5065\ s^{-1}$ and $\beta' = 0.8502\ s^{-1}$. The shared point 9

corresponds to an amplitude of only about 1 mm. The lower-amplitude regime of the exponential decay may occur due to pinning of the liquid at the wall when the amplitude is sufficiently small. This would be a Poiseuille-flow of U-tube oscillations. For our drive threshold data in Section D.1, we had to impart initial amplitudes of roughly 3–5 mm. We thus use the greater-amplitude value $\beta = 0.5065\ s^{-1}$ as the damping parameter for the theoretical values of the threshold amplitude from rest. For the theoretical natural frequency $f_0 = 1.025$ Hz (Section D.1), the quality factor is $Q = \pi f_0/\beta = 6.36$. This typically low value is an ominous indication that high drive amplitudes would be required to achieve parametric excitation of U-tube oscillations.

Note that there is a slight amount of positive curvature in the upper data in Figure 17. This behavior is indicative of weak nonlinear damping, which is greater at larger amplitudes. The slight positive curvature is consistent with a qualitative comment made by Morinigo (1972), and can also be barely seen in the graph by Gilson and Boedtker (1969) if their final data point is ignored.

It is interesting that there exists a different case of U-tube oscillations with a piecewise-linear free decay. The free decay of liquid helium below the temperature for superfluidity exhibits piecewise-linear behavior (Donnelly 1956), although there is a significant transition region between the two linear regimes. The behavior is attributed to the two-fluid model (normal and superfluid), where the two fluids become locked together at the larger amplitudes. The “knee” in the semilog plot bends in the *opposite* direction of our knee in Figure 17, due to a decrease in the lack the damping for the superfluid component. Curiously, it appears to be a coincidence that the knees in both cases occur at approximately the same displacement amplitude (1 mm).

Possible future work is to increase the amplitude in order to more clearly observe and quantify the nonlinear damping (but still keep the ends of the liquid in the vertical sections so that Hooke’s law holds). Other possible future work is to improve the lower-amplitude data by using a greater length of the liquid so that more data can be gathered, and by using a larger-diameter tube so that a two-wire resistive probe can be used to accurately measure the displacement of the liquid as a function of time. Poiseuille-flow theory for a U-tube can be done, and compared to the experimental data to see if this is the

cause of the increased damping parameter. Finally, possible further connections between our classical U-tube and a superfluid U-tube can be explored.

D. DRIVE AMPLITUDE THRESHOLDS

1. Excitation from Rest

In general, parametric excitation of a linearly damped simple harmonic oscillator that is initially at rest in equilibrium only occurs for drive amplitudes above a threshold value that depends upon the drive frequency f and the linear damping parameter β (the amplitude of a free decay is proportional to $e^{-\beta t}$, where t is the time). In addition, because this is an instability, small fluctuations are required for the growth to occur. The dimensionless drive amplitude threshold η_{min} can be analytically determined (Denardo, 2017; Landau & Lifshitz, 1976). Expressed in terms of frequency (rather than angular frequency), which is appropriate for experiments, the relationship is

$$\eta_{min} = \frac{2}{f_0}\sqrt{\left(2f_0 - f\right)^2 + \frac{\beta^2}{\pi^2}}\ , \tag{3.1}$$

where f_0 is the natural frequency of the oscillator. The relationship (3.1) is an approximate one that holds for negligible nonlinearity and weak damping, and for the drive frequency f in a neighborhood of $2f_0$. The relationship corresponds to a hyperbola in the "drive plane" of η_{min} vs. f. Parametric excitation of an oscillator initially at rest and subject to small fluctuations occurs when $\eta > \eta_{min}$. The absolute minimum threshold value corresponds to $f = 2f_0$ in Equation (3.1), which yields

$$\left(\eta_{min}\right)_{abs} = \frac{2\beta}{\pi f_0} = \frac{2}{Q}\ . \tag{3.2}$$

In the final expression, $Q = \omega_0/2\beta$ is the quality factor for small-amplitude oscillations (B. C. Denardo, n.d.; Kinsler et al., 2000), where ω_0 is the natural angular frequency of the oscillator.

For our case in which the acceleration due to gravity is modulated, the

dimensionless drive amplitude is

$$\eta = \frac{a}{g} = \frac{\omega^2 d}{g} = \frac{4\pi^2 f^2 d}{g}, \tag{3.3}$$

where a is the peak acceleration amplitude of the drive, g is the acceleration due to gravity, $\omega = 2\pi f$ is the angular frequency of the drive, and d is the peak displacement amplitude of the drive. For linear oscillations of a U-tube, the natural frequency of a liquid of length L is well-known to be

$$f_0 = \frac{1}{2\pi}\sqrt{\frac{2g}{L}}. \tag{3.4}$$

Setting $\eta = \eta_{min}$ and $d = d_{min}$ in Equation (3.3), substituting the result into Equation (3.1), and solving for d_{min}, yields

$$d_{min} = \frac{g}{8\pi^2 f_0^3}\sqrt{(2f_0 - f)^2 + \frac{\beta^2}{\pi^2}}, \tag{3.5}$$

where we have set $f = 2f_0$ in the factor of the square brackets, due to the assumption that both terms in the square brackets are small. We compare the expression (3.5) to experimental data later in this section. For a final theoretical expression, from Equation (3.5) for $f = 2f_0$, or equivalently from Equations (3.2) and (3.3), the absolute minimum displacement is

$$(d_{min})_{abs} = \frac{g\beta}{8\pi^3 f_0^3}. \tag{3.6}$$

In our initial experiments with a parametrically driven U-tube, we were *not* able to achieve parametric excitation from rest. Fluctuations of the ends of the liquid were small but clearly visible. These were present due to the driver, especially as a result of the distortion at higher amplitudes, which causes a “jerkiness” in the waveform. We naturally thought that the problem was that the excitation required drive amplitudes greater than our

maximum peak value of 1 inch, especially due to the greater damping parameter at small amplitudes (Section 3.C). However, the problem turned out to be that we were not allowing a sufficient amount of time for the instability to occur. We then decided to set a waiting time of 3 minutes for each drive amplitude. If growth was not evident, we repeated the process at a slightly greater amplitude. In a significant number of cases, the growth required 2 minutes or more to occur. These long times offer a dramatic lecture demonstration!

Unfortunately, our second data gathering session yielded significantly different drive amplitude thresholds; that is, the data were not sufficiently repeatable. A possible reason for this behavior is that, near threshold, a sufficient fluctuation that causes the instability to occur may have only rarely occurred during the 3 minute waiting time.

To improve the data-gathering procedure, we attached the food baster (Section 3.C) to one end of a length of small-diameter flexible tubing, and supported the other end with clamps on a tripod such that the end of the tube was directed vertically downward about 1.2 inches above one end of the U-tube (Figure 18). With the drive on, we abruptly and fully squeezed the bulb of the baster, which caused an initial peak displacement amplitude of roughly 3 to 5 mm of the liquid in the U-tube. This “kicking” was repeated several times at each drive amplitude, so that the phasing could possibly lead to growth before the decay prevented this.

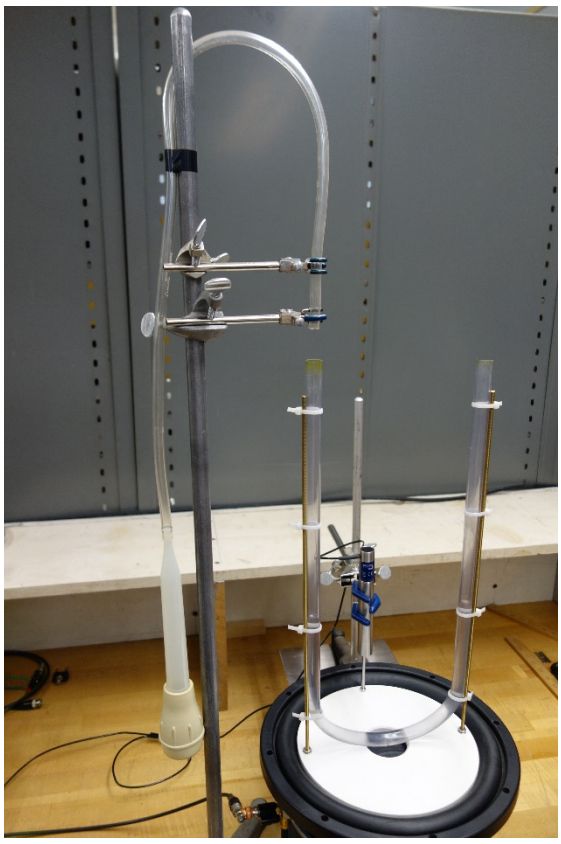

U-tube apparatus with a simple hand air-pulsed method of imparting small-amplitude motion while the U-tube is being driven by the shaker. A food baster is connected with flexible tubing to a point above the left arm of the U-tube.

Figure 18. U-tube Apparatus with a Hand Pump for Displacement.

Much patience was required to obtain even only moderately accurate values of the threshold amplitude. The reason is that a parametric drive, which causes exponential growth, can be roughly considered as counteracting dissipation, which causes exponential decay. In a neighborhood of the threshold, the oscillator is thus roughly free, which means that transient times are very long. Another problem is the significant heating of the voice coil of the subwoofer, which occurs due to the relatively large current required for greater drive amplitudes. The heating increases the resistance which, for constant voltage, lowers the drive amplitude. Of course, the LVDT reading is what is relevant, but this required a long 32-second acquisition time (Section 3.C).

A graph of experimental data for the drive amplitude threshold from near-rest is shown by the upper set of points in Figure 19. The liquid in equilibrium is given small

initial displacements, as described above. The theoretical prediction (3.5) is shown by the solid curve, where we have used an empirical value of f_0. This value could be directly measured by timing oscillations. However, it is more accurately determined from the absolute minimum of the experimental threshold data in Figure 19, which yields approximately $2f_0 = 1.935$ Hz, or $f_0 = 0.9675$ Hz. Once parametric excitation occurs, we observed that the eventual steady-state amplitude is large (on the order of 10 cm) for higher drive frequencies, and low (on the order of 1 cm) for lower drive frequencies. The lower set of data points correspond to the threshold of the maintenance of steady-state oscillations, which is discussed in the next section (Section D.2).

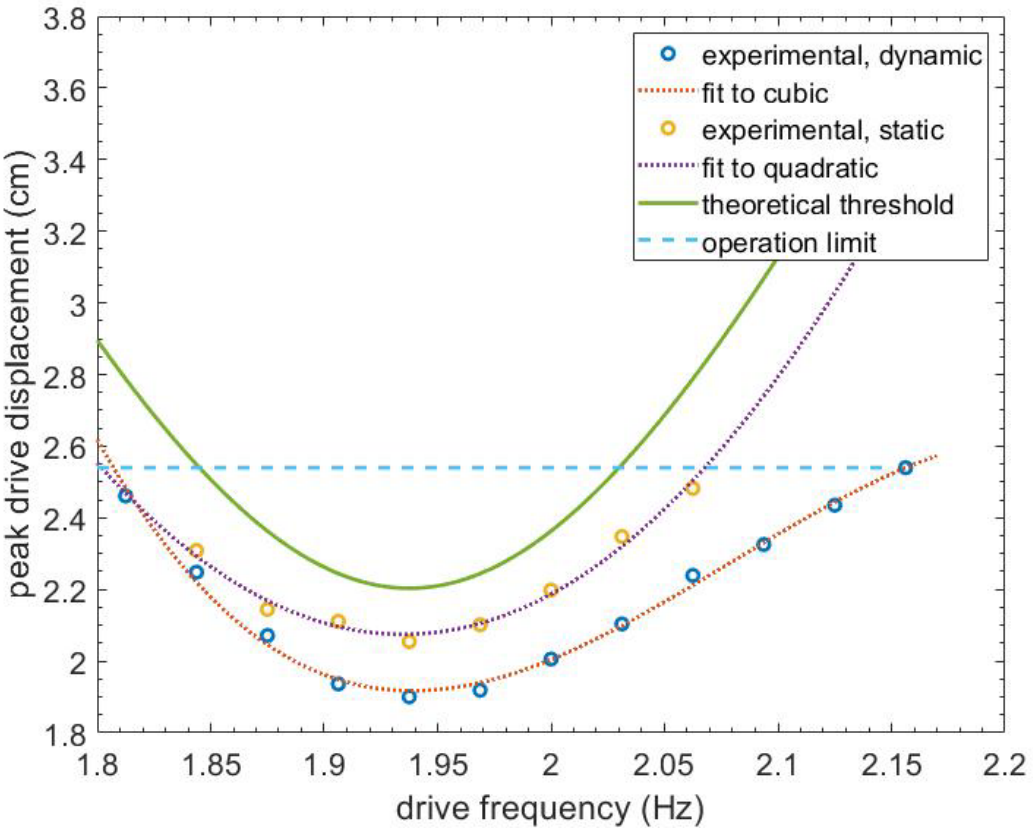

The upper set of experimental data corresponds to excitation from near-rest. The lower set corresponds to maintenance of steady-state oscillations (refer to Section D.2). The solid curve is the theoretical threshold for excitation from rest. The dotted curves are quadratic and cubic curve fits for excitation from rest and maintenance of steady-state oscillations, respectively. The dashed line is the maximum displacement for both the LVDT and the subwoofer.

Figure 19. Drive Amplitude Thresholds as a Function of Drive Frequency.

The theoretical threshold for excitation from rest is systematically greater than the experimental data. We suspect that this occurs due to the 3–5 mm amplitude fluctuation that we imparted while gathering the experimental data (see above). In the future, smaller fluctuations can be imparted to the liquid in order to check whether this increases the measured threshold values.

We can readily quantitatively compare the experimental and theoretical values of the drive frequency at the absolute minimum threshold. The theoretical drive frequency for this case is $2f_0$, where the natural frequency f_0 is given by Equation (3.4). For the length of liquid L = 47.1 cm, the predicted value is $2f_0$ = 2.05 Hz. From the graph, as stated above, the experimental value is approximately 1.935 Hz, which is smaller by 5.6%. The observed value of the natural frequency is expected to be less than the theoretical value f_0 due to the reduction of cross-sectional area of the rounded portions of the tube, for the following reason. Consider a U-tube with a uniform cross-sectional area, and then imagine slowly reducing the cross-sectional area near the bottom by a small amount. Reducing the area must *increase* the maximum kinetic energy because the velocity increases by an amount proportional to the change in area and the mass decreases by the same fractional amount, but the kinetic energy is proportional to the square of the velocity. Because the maximum potential energy remains the same, and the maximum kinetic energy must equal the maximum potential energy by energy conservation, the frequency must *decrease*.

We can also readily quantitatively compare the theoretical and experimental drive displacement amplitudes at the absolute minimum threshold. The theoretical absolute minimum drive amplitude threshold is given by Equation (3.6), which yields $(d_{min})_{abs}$ = 2.21 cm for the empirical natural frequency f_0 = 0.9675 Hz and the damping parameter β = 0.5065 s^{-1} (Section 3.C). The value from the graph of the experimental data is approximately 2.075 cm, which is less than the theoretical value by 6.1%. As explained above, this error is probably due to the fact that the initial amplitude we imparted to the liquid was not sufficiently small.

2. Maintenance of Steady-State Oscillations

The parametric drive amplitude threshold to maintain steady-state oscillations is *distinct* from that for excitation from rest. The steady-state threshold depends upon the nonlinearity that limits the growth, whereas the threshold for excitation from rest in equilibrium only involves linear parameters (Denardo 2017).

Our procedure for measuring the peak amplitude threshold of the displacement drive as a function of drive frequency is as follows. The amplitude of the function generator is set to a sufficiently low value such that the gain on the power amplifier can be turned to maximum. This gives us accurate control of the drive voltage by adjusting voltage of the function generator. To begin, we turn the gain of the power amplifier to zero, and then substantially "kick" (impart an impulse to) the liquid by momentarily inserting the end of a large food baster into one end of the tube and compressing or expanding the bulb of the baster. We then quickly remove the baster and immediately turn the power amplifier completely on. If steady-state oscillations do not occur (that is, if the liquid returns to equilibrium), we repeat the procedure but now with a greater drive amplitude. Eventually, when steady-state oscillations occur, we carefully lower the drive amplitude in sufficiently small increments until the steady-state oscillations cease, and the liquid returns to equilibrium. During this time, we continually monitor the voltage readout of the LVDT on the function analyzer (Section B.1). Applying the calibration factor yields the minimum peak displacement amplitude to maintain the oscillations.

It should be mentioned that the voltage amplitude of the function generator is used as only a very rough guide for where to start our search. The values are not consistent due to the heating of the voice coil of shaker, which causes a reduction in displacement amplitude for a fixed voltage.

We encountered several difficulties in the course of obtaining accurate repeatable data. Extreme patience was required when the drive amplitude was altered, because the relaxation of the response due to a change in the drive amplitude was very slow. This behavior occurred because a parametric drive at threshold can be crudely considered as approximately cancelation the damping, which yields a long transient time. Another

problem, which only eventually became apparent in our effort to obtain repeatable data, was that the evaporation rate of the alcohol greatly increased due to the agitation of the oscillations. Over the time required to obtain only several data points, the length of the alcohol could decrease by roughly 0.2 cm (1 mm drop in either arm). For our length of roughly 50 cm, the resultant fractional increase in natural frequency $f_0 = (1/2\pi)(2g/L)^{1/2}$ is $\delta f_0/f_0 = (1/2)\delta L/L$, which is roughly only 1%. However, this is sufficient to make a noticeable difference due to the frequency scale of the data in Figure 19. As the first step in the process of measuring a data point, we carefully checked the level of the liquid and, if necessary, added alcohol such that the bottom of the equilibrium meniscus in one arm was 1.00 cm above the top of a cable tie.

The final data set is shown in Figure 19 (lower set of data). The dashed line corresponds to the 1-inch peak limitation of both the driver and LVDT, as well as the dial indicator we used to calibrate the LVDT. The clear left-right asymmetry in the data is apparently due to the fact that the relevant parametric drive amplitude is proportional to the acceleration $\omega^2 d$ rather than displacement d. Specifically, for frequencies on the right side, the displacement threshold is expected to be less than that on the left side, which is observed. Due to time limitations, we did not measure the steady-state amplitudes. Qualitatively, the amplitudes were large (on the order of 10 cm) at higher frequencies and small on the order of 1 cm) at lower frequencies. This behavior is again qualitatively consistent with the relevant drive being acceleration rather than displacement.

By far the most important and surprising aspect of the steady-state threshold data in Figure 19 is that it apparently occurs for *linear* oscillations of the liquid in the U-tube. Specifically, the ends of the liquid do not enter the rounded portion of the U-tube, and the dissipation is nearly linear (Section 3.C). Parametric growth is only limited by a nonlinearity, so what is limiting the growth in our U-tube? It is possible that the small amount of nonlinearity of the dissipation is responsible, and this could be established by comparing calculations and measurements. The only other possible source is the driving mechanism. The liquid has mass. As its amplitude grows, the reaction on the drive increases. An ideal drive, which is very often assumed in theory, maintains its amplitude regardless of the response of an oscillator. Realistically, however, the drive amplitude

decreases, which can lead to limitation of the parametric growth. An extreme example is a parametric instability, in which one mode of a system parametrically drives another (Section 3.A). In that case, energy conservation dictates that the amplitude of the driving mode must decrease as the amplitude of the driven mode increases. Possible future work is to search the literature and, if necessary, develop a theory in which the nonideal nature of a parametric drive limits the growth. That our U-tube data threshold data for steady-state motion is well-fit with a simple cubic polynomial suggests that an approximate theory might be straightforward.

E. CONCLUSIONS AND FUTURE WORK

Parametric excitation has very different properties compared to the standard case of a directly-driven oscillator. Although parametric excitation is usually not taught is classes, it still can and should be discussed with demonstrations, especially because it can cause a dangerous instability in the motion of ships. We have achieved steady state parametric excitation of U-tube oscillations, which has not previously been reported in the literature, and our apparatus is appropriate as a classroom demonstration. We adapted a subwoofer (low-frequency high-amplitude loudspeaker) as a vertical shaker to modulate gravity in the frame of reference of the U-tube. The drive amplitude was measured with an LVDT (linear variable differential transformer) which we carefully calibrated. The damping parameter for oscillations of our U-tube was determined from free decay measurements. The parametric drive amplitude threshold, which depends upon the damping parameter, is in rough agreement with theory, and have we qualitatively explained the deviation.

Our observations have surprisingly uncovered two fundamental unresolved issues regarding U-tube oscillations. The logarithmic free decay of the amplitude of the oscillations as a function of time yields *two* different slopes (damping parameters): one for small amplitudes equal to or less than roughly 1 mm, and one for greater amplitudes. In addition, the nature of the nonlinearity that limits the exponential parametric growth in our U-tube is not yet known. However, it is *not* a breakdown of Hooke's law, which typically limits the growth in the case of parametrically driven pendulums and other systems.

There is a substantial amount of future work that can be done. One topic, which is interesting and related to parametric excitation for small fluctuations from equilibrium, involves the small-amplitude free decay of U-tube oscillations. A greater number of data points are needed to accurately and convincingly establish the small-amplitude damping parameter. This could be accomplished by using a U-tube with a greater cross-sectional area, which both increases the quality factor (and thus the number of oscillations) and allows the space for a sensitive two-wire resistive probe to accurately measure the amplitude. A Poiseuille-flow theory should be compared to the experimental data, to determine whether this theory accounts for the damping parameter.

At the other extreme, greater amplitudes of the free-decay should be measured in order to quantify the slight nonlinear dissipation. The literature should be searched for a general theoretical calculation of nonlinear dissipation limiting the growth of parametric excitations. If such a theory does not exist, it should be formulated. The results can then be used to quantitatively conclude whether or not this nonlinearity is limiting the growth in the case of parametrically-excited U-tube oscillations.

If the nonlinear dissipation does not account for the steady-state motion, the only other possibility appears to be that the motion of the liquid reduces the drive amplitude. An attempt should be made to measure the reduction in drive amplitude. In addition, a search of the scientific literature on such a nonideal drive should be performed. If no research is found, a theory should be done and then compared to experimental data.

Other future work is to use video to measure the parametric growth of the amplitude and the eventual steady-state amplitude. This would be dramatic when driving just above threshold. Excitation would be visually apparent only after a time on the order of many seconds or even minutes, after which the growth accelerates. There are two possible reasons for the behavior. Either the growth is extremely slow ($e^{\beta t} = 1 + \beta t$, for $\beta t << 1$), or there is actually no growth until it is initiated by a small fluctuation. Experiments could resolve this issue. If the time for noticeable growth significantly varies, then the latter is probably occurring. It is also possible to use a sensitive two-wire resistive probe to accurately observe the behavior.

Use of a subwoofer as a shaker has a number of disadvantages. The maximum excursion (typically 2 inches peak-to-peak) is not sufficient to fully probe the behavior of a parametrically driven U-tube. Indeed, only with careful experimentation were we able to "eke out" a limited amount of threshold data. In addition, for greater drive amplitudes, the heating of the voice coil causes a reduction of amplitude for a fixed voltage. This effect, together with the long acquisition time of the signal analyzer, substantially hinders the gathering of accurate data. Finally, the subwoofer could be the responsible for limiting the parametric exponential growth of the oscillations. An alternative low-frequency shaker that operates by the conversion circular motion of a dc motor to rectilinear simple harmonic motion could be made. A problem, however, is that the drive amplitude can only be altered by stopping the motor and changing the radial distance of the connecting arm to the motor. This operation would substantially increase the time required to take data, but the benefits could well outweigh the disadvantage.

Finally, glass U-tubes can be made by heating, bending, and tempering a straight tube. Glass may have some advantages over Tygon tubing. For example, the quality factor may be greater, and the rigidity of glass would beneficial if a two-wire surface height probe is inserted in the tube. A disadvantage of glass may be that the cross-sectional area in the bent regions is more greatly reduced, which could result in turbulence.

THIS PAGE INTENTIONALLY LEFT BLANK

IV. SUMMARY

Lecture demonstrations can play an important role in physics education, especially in our age of STEM. Because demonstrations are nearly always done with actual physical systems, realistic effects that are beyond a simple theory often arise, and lead to classroom discussions. Scholarly investigations of demonstrations are part of educational research, which includes quantitative experiments and theoretical analysis to confirm explanations. The results can be surprising. This thesis presents investigations of two possible lecture demonstrations: the two-bullet problem, and parametric excitation of U-tube oscillations. Surprising results occurred in both of these investigations, as summarized in the sections below.

A. TWO-BULLET PROBLEM

A body is released from rest at some height above the floor. At the same time, a second body is projected horizontally. When drag due to the air is negligible, it is well-known and elementary to show that both bodies strike the floor at the same time. This behavior occurs regardless of the nature of the bodies and the value of the initial velocity of the projected body. For identical bodies, when the drag is not negligible and is modeled to be quadratic in the velocity, it is not difficult to show that the dropped body must strike the floor first. Can this be convincingly demonstrated?

Our investigations show that the answer is currently *no*. If steel balls in one type of commercial apparatus are replaced by Styrofoam balls of roughly the same diameter, and the demonstration is performed, the dropped ball clearly strikes the floor before the projected ball. The time difference is approximately 0.2 s. However, computer simulations surprisingly show that it is impossible to a have a classroom demonstration in air, where the time difference is qualitatively discernible and the downward acceleration is the acceleration due to Earth's gravity. The reason for this behavior is not obvious and cannot be simply stated (refer to Section 2.C.1). The demonstration is suspect because the apparatus imparts a substantial spin to the projected body, causing it to noticeably curve horizontally due to the Magnus force. Although this spin appears to be only about the

vertical axis, there may be a horizontal component which could cause a lift force, or the spin about the vertical axis could conceivably cause a small secondary Magnus lift force. Computer simulations show that buoyancy effectively reduces the acceleration due to gravity, and can lead to a discernible time difference, but the bodies must be nearly neutrally buoyant. Buoyancy does *not* account for our experimental observation of a 0.2 s time difference.

An experiment was done with actual but unspecified bullets in a TV episode of MythBusters. The dropped bullet struck the floor 0.04 s before the fired bullet. MythBusters attributed this to experimental error, but our simulations indicate that roughly one-fourth of the time difference was due to the quadratic drag effect.

Future work includes modifying a second type of demonstration apparatus to simultaneously drop and launch the Styrofoam balls. In this case, *no* spin is imparted to the projected ball. The balls should strike the floor with no discernible time difference. Also interesting would be to understand why the first apparatus yields a discernible time difference. High-speed video could reveal if a reverse top spin is present, which would cause a lift force that is responsible for the delayed time-of-flight of the projected ball. If there is no such spin to investigate the possibility of a secondary Magnus force, this would be of fundamental importance in fluid mechanics.

Other future work involves graphically quantifying the effect of buoyancy (effectively, a reduced gravitational acceleration) on the time difference. It would be remarkable if there is *no* known planet or moon on which the demonstration could be successful. Note that both the gravitational effect and drag due to the atmosphere would need to be included.

Finally, the possibility of a table-top aquarium with a small drop-launch mechanism with various types of balls should be explored. Buoyancy could be utilized here. However, it is important to check that the drag is not in the linear regime, because linear drag does *not* cause a time difference.

More detailed statements of our conclusions and future work on the two-bullet problem are in Section 2.D.

B. PARAMETRIC EXCITATION OF U-TUBE OSCILLATIONS

Excitation of pendulum oscillations by vertically oscillating the support is an example of *parametric excitation*. This demonstration is readily done by hand if the drive frequency is approximately twice the natural frequency of the pendulum. A similar situation occurs when waves strike a ship. If the resultant vertical oscillations have approximately twice the frequency of the rolling oscillations, large amplitude rolling can occur, which has caused extensive damage.

If a U-tube that is partially full of a liquid is vertically driven at approximately twice the frequency of the liquid oscillations, we would expect these oscillations to occur. However, this is unlikely, as we experienced. The reason is that parametric excitation only occurs when the drive amplitude exceeds a threshold value which increases for greater damping, and U-tube oscillations are typically substantially damped.

It is natural to then ask why parametric excitation of U-tube oscillations should be attempted at all. Our motivation lay in the fact that parametric excitation has the property that only a nonlinearity can limit the growth of the oscillations, leading to a steady-state response. There are two possible nonlinearities of U-tube oscillations: a breakdown of Hooke's law when the liquid enters the rounded portions of the U-tube, and nonlinear dissipation (the resistive force not being proportional to the velocity). We found that the latter only occurs very weakly in our U-tube. A dramatic demonstration would then be to drive the U-tube just above threshold, which would cause an initially slow growth which would accelerate and then reach a steady state where ends of the liquid encounter the rounded portions. This would be visual proof that nonlinearity limits the growth of parametric excitation.

However, our observations surprisingly show that the steady-state motion occurs *before* the liquid enters the rounded portions. The only other possible nonlinearity appears to involve the lack of an ideal driving mechanism; specifically, the response of the liquid reacting back onto the drive, causing a reduction of the drive amplitude.

Another surprising observation is that *two* different decay parameters occur for the free-decay of U-tube oscillations, although one of these occurs only for amplitudes that are

roughly 1 mm or less. Remarkably, a similar phenomenon occurs for the free decay in a superfluid liquid helium U-tube for roughly the same amplitudes, although the reason does not appear to be related to classical U-tubes. The occurrence in our case may be that there is a transition to Poiseuille flow as the amplitude decreases.

Future U-tube work includes a variety of topics. The nonlinearity that limits the parametric growth must be understood, and the free-decay data for small amplitudes must be improved and compared to Poiseuille theory. In addition, the growth and steady-state motion should be measured, including the initial growth at small amplitudes. The subwoofer that we use as a drive should be replaced with a dc motor whose motion is converted to one-dimensional simple harmonic motion, and glass rather than Tygon tubing should be used for a U-tube.

More detailed statements of our conclusions and future work on U-tube oscillations are in Section 3.E.

APPENDIX. EULER'S METHOD SIMULATION

Euler's method simulation of two bullet problem for projectile using MATLAB.

```
clear
clc
close all
tic
%% Intialization
Hi = 2; %m              % Initial Height
C= 0.295;               % Drag coefficient bullet
m= 15E-3; %kg           % mass bullet
d= (11.5E-3); %m        % Diameter Bullet
v0= 255; %m/s           % Bullet Initial Velocity
dt=1/10000000; %s       % Time Step
g=9.81; %m/s^2          % Acceleration of gravity
rho0=1.225;             % Air density at sea level (kg/m^3)
r = d/2; %m             % Radius Bullet
A=pi*r^2;               % Cross-section area (m^2)
gamma=C*rho0*A/(2*m);   % Drag parameter
%% Loops
Td2 = 1/sqrt(gamma*g) * acosh(exp(gamma*Hi)); %real drop case
x1= 0; y1= Hi; %y1= Hi(i);         % Initial distance, height drop case
vx1= 0;                  % Initial x-velocity drop case
vy1= 0;                  % Initial y-velocity drop case
t1= 0;                   % Time of flight drop case
while y1>=0
    x1=x1+vx1*dt;
    y1=y1+vy1*dt;
    v=sqrt(vx1^2+vy1^2);
    vx1=vx1-gamma*v*vx1*dt;
    vy1=vy1-gamma*v*vy1*dt-g*dt;
    t1=t1+dt;
end
Td= t1;
x2=0; y2=Hi;        % Initial distance, height projectile case
vx2=v0;             % Initial x-velocity projectile case
vy2=0;              % Initial y-velocity projectile case
t2=0;               % Time of flight projectile case
%% Simulate trajectory (Euler method)
while y2>=0
    x2=x2+vx2*dt;
    y2=y2+vy2*dt;
    v=sqrt(vx2^2+vy2^2);
    vx2=vx2-gamma*v*vx2*dt;
    vy2=vy2-gamma*v*vy2*dt-g*dt;
    t2=t2+dt;
end
R=x2-y2*vx2/vy2;
Tp= t2;
DelT= Tp-Td;
toc
```

THIS PAGE INTENTIONALLY LEFT BLANK

LIST OF REFERENCES

3B Scientific. (2019). Drop and launch apparatus—Vertical and horizontal trajectories. 3B Scientific. https://www.a3bs.com/drop-and-launch-apparatus-1000588-u119831-3b-scientific,p_574_14951.html

Burris, J. L., Hester, B. C., & Mamola, K. C. (2018). The two-bullet problem with constant magnitude drag force. *The Physics Teacher*, *56*(6), 350–343.

Denardo, B. C. (2017). Direct drive and parametric. In Nonlinear Oscillations and Waves: An Introduction with Demonstrations.

Denardo, B., Earwood, J., & Sazonova, V. (1999). Parametric instability of two coupled nonlinear oscillators. *American Journal of Physics*, *67*, 187–195. https://doi.org/10.1119/1.19225

Donnelly, R. J., & Penrose, O. (1956). Oscillations of Liquid Helium in a U-Tube. *Physical Review*, *103*(5), 1137–1144. https://doi.org/10.1103/PhysRev.103.1137

Emerson, S. (2015). *Development of physics lecture demonstrations* [M.S. physics thesis]. Naval Postgraduate School.

Garlington, K., & Martinez, M. (2017). Educational physics demonstrations: outreach project proposal, slinky wilberforce oscillator, and wilberforce pendulum lattice [M.S. physics thesis, Naval Postgraduate School].

Gilson, J. E., & Boedtker, O. A. (1969). A damped harmonic motion experiment for use in undergraduate general physics laboratories. *American Journal of Physics*, *37*(11), 1157–1158. https://doi.org/10.1119/1.1975234

Keeports, D. (1997). Drag and the two-bullet problem. *The Physics Teacher*, *35*(3), 188–191. https://doi.org/10.1119/1.2344638

Khan, F. (2015). Development of physics lecture demonstrations for undersea warfare curriculum [M.S. physics thesis]. Naval Postgraduate School.

Kinsler, L. E., Frey, A. R., Coppens, A. B., & Sanders, J. V. (2000). *Fundamentals of acoustics* (4th ed.). Wiley.

Landau, L. D., & Lifshitz, E. M. (1976). Section 27. *Mechanics* (3rd ed., Vol. 1). Butterworth-Heinemann.

Michaelis, M. M., & Woodward, T. (1991). An inverted liquid demonstration. *American Journal of Physics*, *59*(9), 816–821. https://doi.org/10.1119/1.16839

Morinigo, F. B. (1972). Fluid oscillations in a u tube. *American Journal of Physics*, *40*(2), 350–351. https://doi.org/10.1119/1.1986533

Neves, M. A. S., & Rodríguez, C. A. (2007). Influence of non-linearities on the limits of stability of ships rolling in head seas. *Ocean Engineering*, *34*(11), 1618–1630. https://doi.org/10.1016/j.oceaneng.2006.11.010

Office of Naval Research. (n.d.). Naval STEM. Office of Naval Research Science and Technology. Retrieved May 13, 2020, from https://www.onr.navy.mil/en/Education-Outreach/naval-stem

Science Source. (1856). "Michael Faraday Delivering Christmas Lecture" Science Source. Retrieved May 13, 2020, from https://www.sciencesource.com/archive/Michael-Faraday-Delivering-Christmas-Lecture--1856-SS2738360.html#/SearchResult&ITEMID=SS2738360

Taylor, J. R. (2005). *Classical mechanics*. Sausalito, Calif: University Science Books.

Pasco. (2019). Drop shoot demo. Pasco. Retrieved October, 2019.

USNA Admissions. (n.d.). Summer STEM. Retrieved May 13, 2020, from https://www.usna.edu/Admissions/Programs/STEM.php

INITIAL DISTRIBUTION LIST

1. Defense Technical Information Center
   Ft. Belvoir, Virginia

2. Dudley Knox Library
   Naval Postgraduate School
   Monterey, California